AN INTERPRETATION OF GRAVITY AND AEROMAGNETIC SURVEYS OF THE GREATER JIDDAH AREA, KINGDOM OF SAUDI ARABIA

BY
MARK E. GETTINGS AND GORDON E. ANDREASEN

OPEN-FILE REPORT
USGS-OF-03-31

MINISTRY OF PETROLEUM AND MINERAL RESOURCES
DEPUTY MINISTRY FOR MINERAL RESOURCES
JIDDAH, KINGDOM OF SAUDI ARABIA
1403 AH 1983 AD

AN INTERPRETATION OF GRAVITY AND AEROMAGNETIC SURVEYS OF THE GREATER JIDDAH AREA, KINGDOM OF SAUDI ARABIA

by

Mark E. Gettings and Gordon E. Andreasen

OPEN-FILE REPORT USGS-OF-03-31

Ministry of Petroleum and Mineral Resources
Deputy Ministry for Mineral Resources
Jiddah, Kingdom of Saudi Arabia
1403 AH 1983 AD

An Interagency Report prepared by the
U.S. Geological Survey
Saudi Arabian Mission
for the
Ministry of Petroleum and Mineral Resources
Kingdom of Saudi Arabia

The work on which this report was based was performed in accordance with a cooperative agreement between the U.S. Geological Survey and the Ministry of Petroleum and Mineral Resources.

The quadrangle identification method used in U.S. Geological Survey Saudi Arabian Mission reports is shown below.

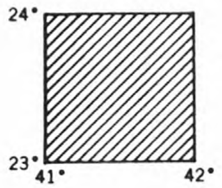

23/41

1-degree quadrangle

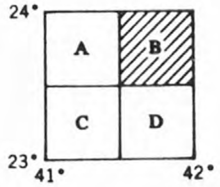

23/41 B

30-minute quadrangle

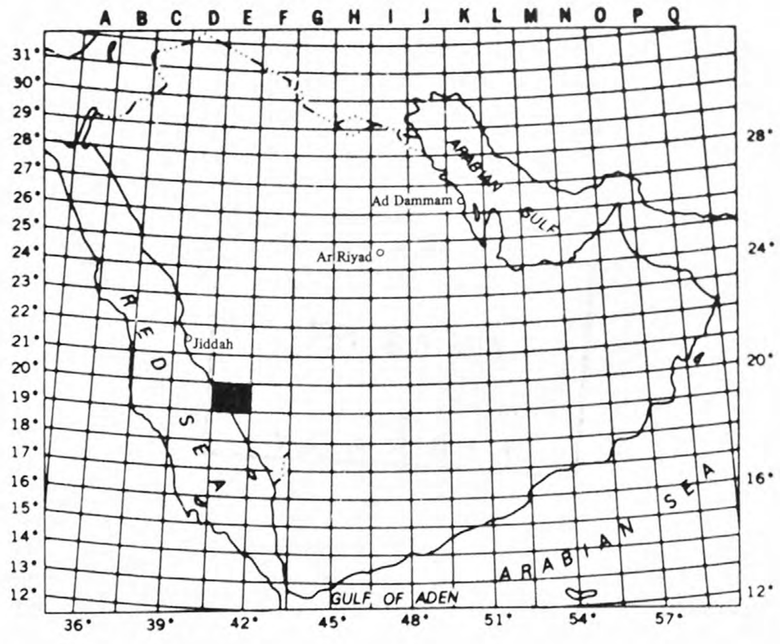

19E

1x1½-degree quadrangle

CONTENTS

ILLUSTRATIONS
[Plates are in pocket]

TABLES

AN INTERPRETATION OF GRAVITY AND AEROMAGNETIC SURVEYS OF THE GREATER JIDDAH AREA, KINGDOM OF SAUDI ARABIA

by

Mark E. Gettings and Gordon E. Andreasen[1]

ABSTRACT

A gravity survey of the Jiddah area between lat 21°23' and 21°48' N., long 39°03' and 39°20' E., carried out in early 1977, covers an area of 744 km^2 and includes 215 stations, at an average spacing of 1.9 km. The resulting simple Bouguer gravity anomaly map shows a series of four large (7-15 mgal) gravity anomaly highs along a north-trending gravity gradient located immediately west of outcrops of Precambrian rocks. The regional Bouguer gravity anomaly field of the map area decreases eastward at an approximately constant rate of about 1.1 $mgal\text{-}km^{-1}$. Several anomalies suggest northeast-trending, right-lateral strike-slip faulting throughout the area.

Interpretation of the Bouguer gravity anomaly map, combined with geologic, aeromagnetic, and paleomagnetic data, leads to an interpretive model in which the gravity gradient marks the boundary zone between Precambrian continental crust to the east and oceanic sea-floor crust overlain by marine sedimentary rocks to the west. The strike-slip faults in the area are probably the landward extension of offshore Red Sea transform faults, and, because they penetrate and offset continental crust, their study may yield useful information about the mechanism of transform faulting. The gravity anomaly highs are interpreted to result from shallow intrusive bodies, probably gabbroic in composition, that are buried a few hundred meters below the surface and that are approximately 2 km thick.

---

[1] U.S. Geological Survey, Reston, VA

INTRODUCTION

We present here the results of a survey made in 1977 to map the gravity field of the greater Jiddah area (fig. 1). The survey was undertaken in an effort to delineate the subsurface geology of the Jiddah area for both regional geologic and engineering geologic studies. An interpretation of the resulting gravity map (plate 1) and the total-intensity aeromagnetic map (plate 2) suggests that there are several major intrusive bodies at the Tertiary-Precambrian boundary (plate 3). These may be related to Red Sea rifting in a manner similar to the relations observed in southern Saudi Arabia on the Tihamat Asir, where intrusions with similar geophysical signatures are exposed (Gettings, 1977).

We wish to acknowledge the help of H. R. Blank and D. L. Schmidt, who participated in valuable discussions and field trips, and the help of Abdullah Showail, who carried out the paleomagnetic determinations in the laboratory. The staff of the U.S. Geological Survey (USGS) Geophysics group, Jiddah, recorded base-station altimetry readings at the USGS office. F. J. Fuller constructed an accurate grid on the photomosaic base. A. J. Petty compiled the aeromagnetic map and, assisted by Said Al-Ghamdi, drew the final gravity and aeromagnetic maps. L. Cordell, M. D. Kleinkopf, and K. K. Kellogg critically reviewed the manuscript and made many valuable suggestions. The work on which this report was based was performed in accordance with an agreement between the U. S. Geological Survey and the Ministry of Petroleum and Mineral Resources, Kingdom of Saudi Arabia.

DATA STORAGE

No entries in the Mineral Occurrence Documentation Systems (MODS) data bank were made or updated as a result of this study, and no base data files were established for this report.

SURVEY DESCRIPTION

The greater Jiddah survey area is between lat 21°23' and 21°48' N., long 39°03' and 39°20' E, and is about 744 km^2 in area; it lies parallel with the Red Sea coast and is roughly rectangular, having dimensions of approximately 17.5 km in the east-west direction and approximately 43 km in the north-south direction. Those offshore islands located at appropriate intervals for the station spacing were included in the survey. A total of 215 gravity stations, 214 of which were established by this survey, were used in the construction of the resulting Bouguer gravity anomaly map.

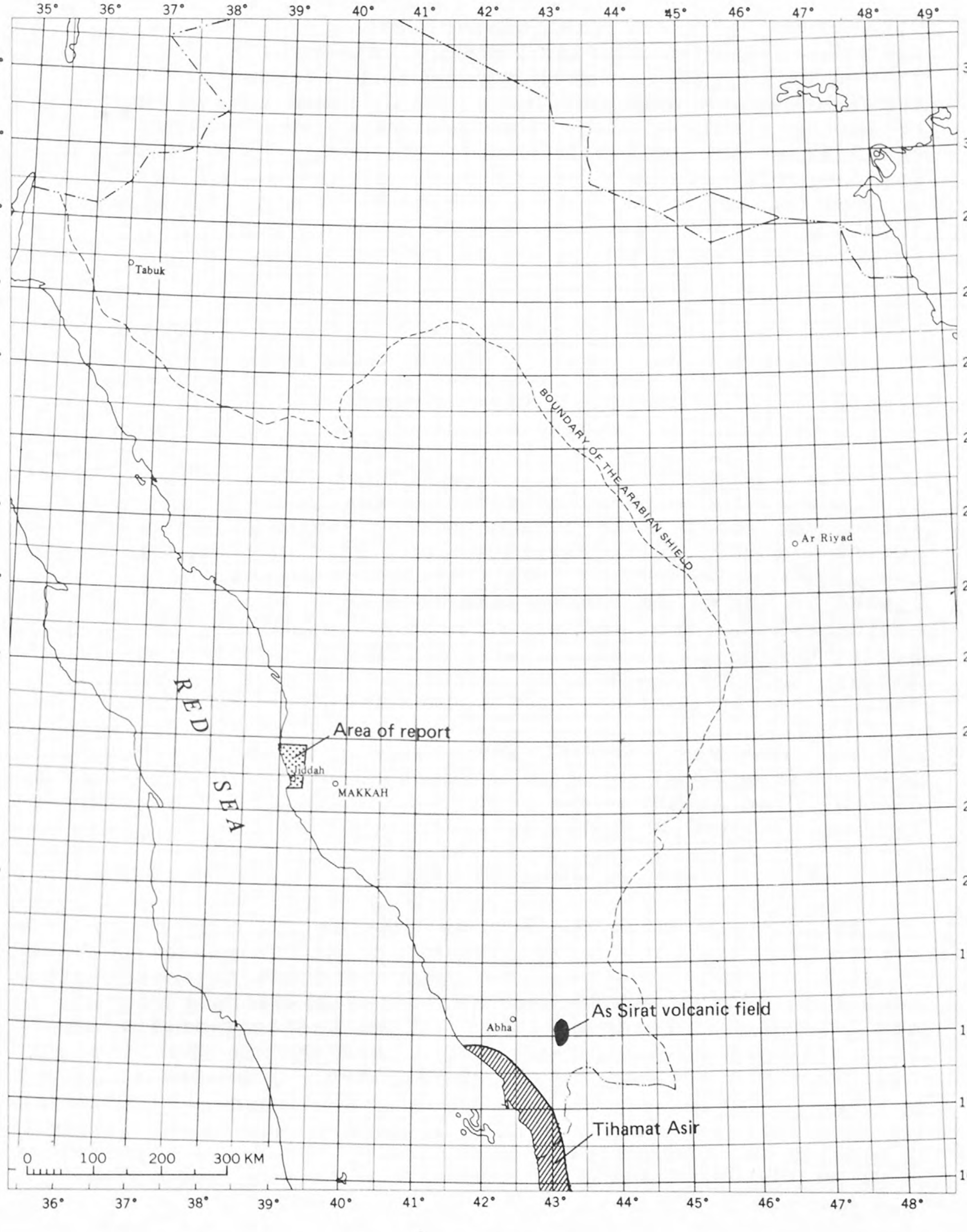

Figure 1.--Index map of western Saudi Arabia showing location of the area of report.

The target spacing between stations was 2 km on a square-grid network oriented parallel with the Red Sea coast. The resulting average area per station was approximately 3.5 km^2, yielding a nominal station spacing of 1.9 km. Both ground and air (helicopter) transport were used. The fieldwork was done during several intervals between January 23 and May 6, 1977. Most survey work was done between 0700 and 1400, and stations were established in closed loops beginning and ending on the temporary gravity base station "USGS X" at the USGS main office in Jiddah. All gravity survey fieldwork was carried out by G. E. Andreasen, assisted by M. Bazzari and others from the USGS Geophysics group, who recorded altimetry observations at the stations. LaCoste and Romberg gravity meters G328 and G330 were used for the survey[1/]. Both meters performed satisfactorily during the course of the survey with no major tares.

Elevation control was established using two pairs of Wallace and Tiernan altimeters; one pair was read at the gravity stations, and another pair was read at half-hour intervals at the USGS office, Jiddah, to determine barometric pressure variations. A Paulin microbarograph was also used to record barometric pressure variations at the USGS office. Most survey loops included a tie to sea level at some station within the loop. Flight planning and navigation were carried out on 1:16,000-scale aerial photography completed in December 1976 by the USGS. When stations were actually established in the field, their locations were pinpricked on these photographs. The horizontal-control grid was provided by F. J. Fuller, who used existing control points on an approximately 1:30,000 scale photomosaic of the greater Jiddah area made by Fairey Surveys, Limited, in 1971.

All observed gravity values were tied to the temporary gravity base station "USGS X" located at the USGS office in Jiddah. The observed gravity of this station (Potsdam datum) is 978,753.580±0.050 milligals (mgals).

DATA REDUCTION

Field data were reduced by use of a computer program written for the Directorate General of Mineral Resources PDP-11/45 computer. The observed meter readings at each station were first corrected for earth-tidal variations according to the formulae of Longman (1959). Then a linear-drift correction, determined from the closure readings on the base station for each gravity loop, was applied. The datum for all

---

[1/]Mention of specific tradenames or products in this report in no way constitutes an endorsement or recommendation.

observed gravity values is relative to the 1930 Potsdam value. Gravity ties to the International Gravity Standardization Network 1971 (IGSN71) were not available at the time of this work.

The gravimeter-drift curves for the survey period are shown in figure 2. For the period January 23 to April 28, 1977, gravimeter G330 had a total cumulative drift of 2.23 mgals, with an uncertainty of 0.29 mgals in the total drift. The average drift rate was 0.181 mgals/day for this meter. For the period May 1 to May 6, 1977, gravimeter G328 had a total cumulative drift of 0.39 mgals, with an uncertainty of 0.039 mgals. The average drift rate was 0.176 mgals/day for this meter. These drift rates amount to approximately 5 mgals/month and are typical for gravimeters in a helicopter-borne operation. Both meters were carried in their standard carrying cases; special vibration-absorption mountings were not used.

Latitude and longitude values were determined by use of measurements from the 1:30,000-scale latitude-longitude grid. Altimetric elevations were determined by reduction of the observed data using the HP9830A computer programs described by Gettings (1979) and Donzeau (1979). When possible, elevations were checked against available map elevations in the Jiddah area.

The Bouguer anomaly values were calculated by use of the DGMR PDP-11/45 computer and standard reduction equations (see Blank and others, 1980, appendix 1). Theoretical gravity values on the spheroid were computed by use of the International Gravity Formula of 1930 in accordance with the base station datum used. A Bouguer reduction density of 2.67 g-cm^{-3} was used. The principal facts for all gravity stations of the survey are presented in the appendix. No terrain corrections were calculated in the reduction of the data for this survey. Because of the very low relief in the survey area, the standard terrain corrections for all stations in the area would be almost constant and thus would offset the Bouguer gravity anomaly values but not significantly alter the shape of the resulting Bouguer gravity anomaly map.

Station locations pinpricked on the aerial photographs are probably accurate to $\pm$10 m. Because the amount of uncertainty in the latitude-longitude grid is unknown, an uncertainty in the latitude and longitude values of approximately 10 m was assumed for the reduction and reflects on the uncertainty in location on the photographs. The major element of uncertainty in the Bouguer anomaly values results from the uncertainty in the elevations at the stations. For this survey, the maximum probable error for a station elevation is approximately $\pm$3.5 m. The average probable error for all

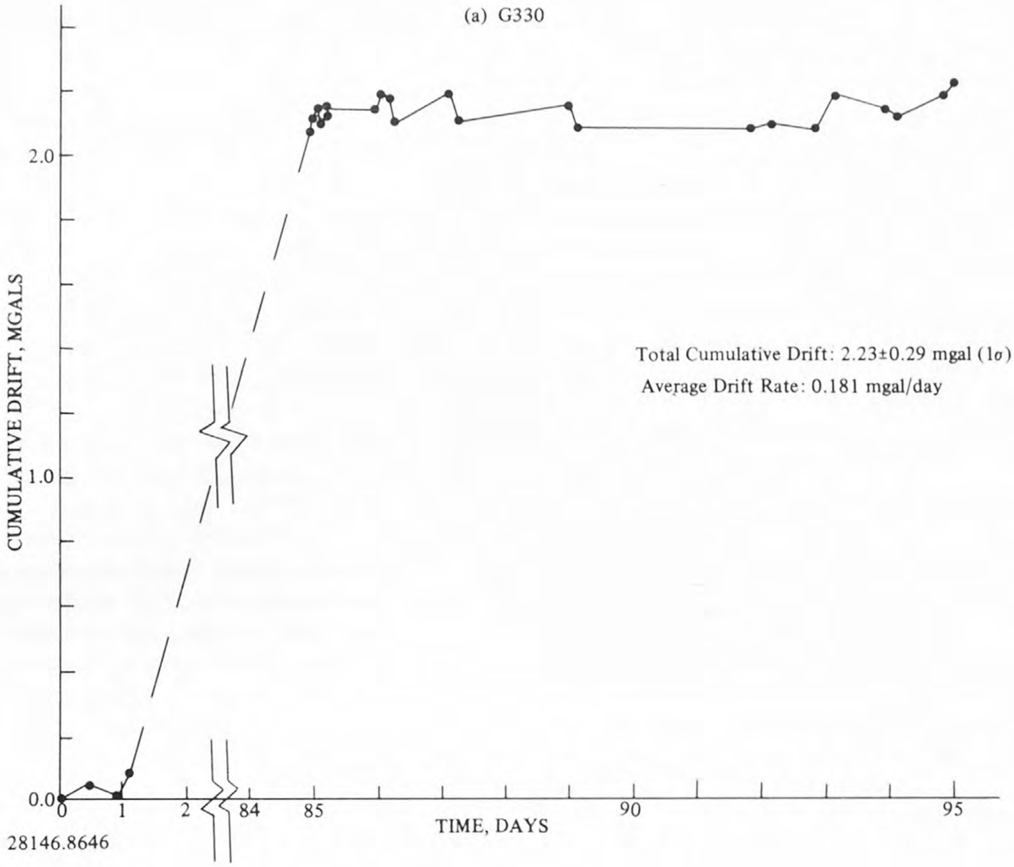

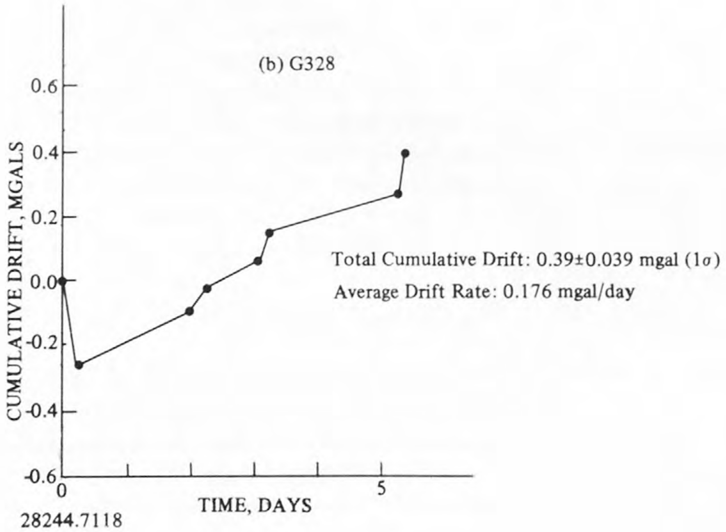

Figure 2.--Graphs showing drift curves for the two LaCoste-Romberg gravimeters used in the survey. The number below the zero of the time axis is the number of days since 1200 hours, December 31, 1899, and defines the time axis in absolute time. Figure (a) is for LaCoste-Romberg gravimeter G330, used for the major part of the survey; (b) is for LaCoste-Romberg gravimeter G328.

stations in the survey is ±1.15 m. For observed gravities, the standard deviation is approximately 0.12 mgal. These uncertainties correspond to a standard deviation for the Bouguer gravity anomaly of about 0.5 mgal. This uncertainty implies that a 1-mgal contour interval is acceptable for a map of the Bouguer gravity anomaly field; the resulting simple Bouguer gravity anomaly map is presented in plate 1.

QUALITATIVE INTERPRETATION

General features and regional trends of the gravity anomaly map

The major features of the Bouguer gravity anomaly map are shown in figure 3, which is a reduced version of plate 1. The larger, discrete gravity anomalies are labeled from 1 to 8, and the more important curvilinear features are labeled from L1 to L5.

Gravity anomaly 1 on figure 3 is open to the north and probably has as its source an intrusive body inferred from a large aeromagnetic anomaly (Arabian Geophysical and Surveying Company, 1976a, sheet 14). Anomaly 2 is a weak, linear, positive anomaly with an amplitude of a few milligals; it correlates well with a corralline limestone outcrop (Morris, 1975) that probably has a positive density contrast with the unconsolidated alluvium to the east. This alluvium constitutes a clastic wedge of debris that has weathered from the low-lying hills of Precambrian bedrock farther to the east and is responsible for gravity anomalies 3 and 4; however, as shown below, the amplitude of these closed lows is reduced by removal of the regional gradient.

Anomalies 5 through 8 are large, positive gravity anomalies with amplitudes ranging from 7 to 15 mgals. They correlate for the most part with unconsolidated alluvium but are associated with some bedrock outcrops (see plate 3). Because these anomalies are all positive with respect to the average of the Bouguer gravity anomaly field associated with the Precambrian outcrops, they must represent material more dense than the exposed Precambrian rocks, which are predominantly dioritic to granitic in composition. Further, because of the rather steep gradients that form the flanks of these anomalies, their sources must be relatively shallow. For an initial interpretation, we postulate that anomalies 5 through 8 are caused by mafic intrusive bodies whose upper surfaces reach quite shallow depths.

Several linear or curvilinear features have been labeled on figure 3, the most dominant of which is the gradient labeled L1. This gradient divides the western coastal plain,

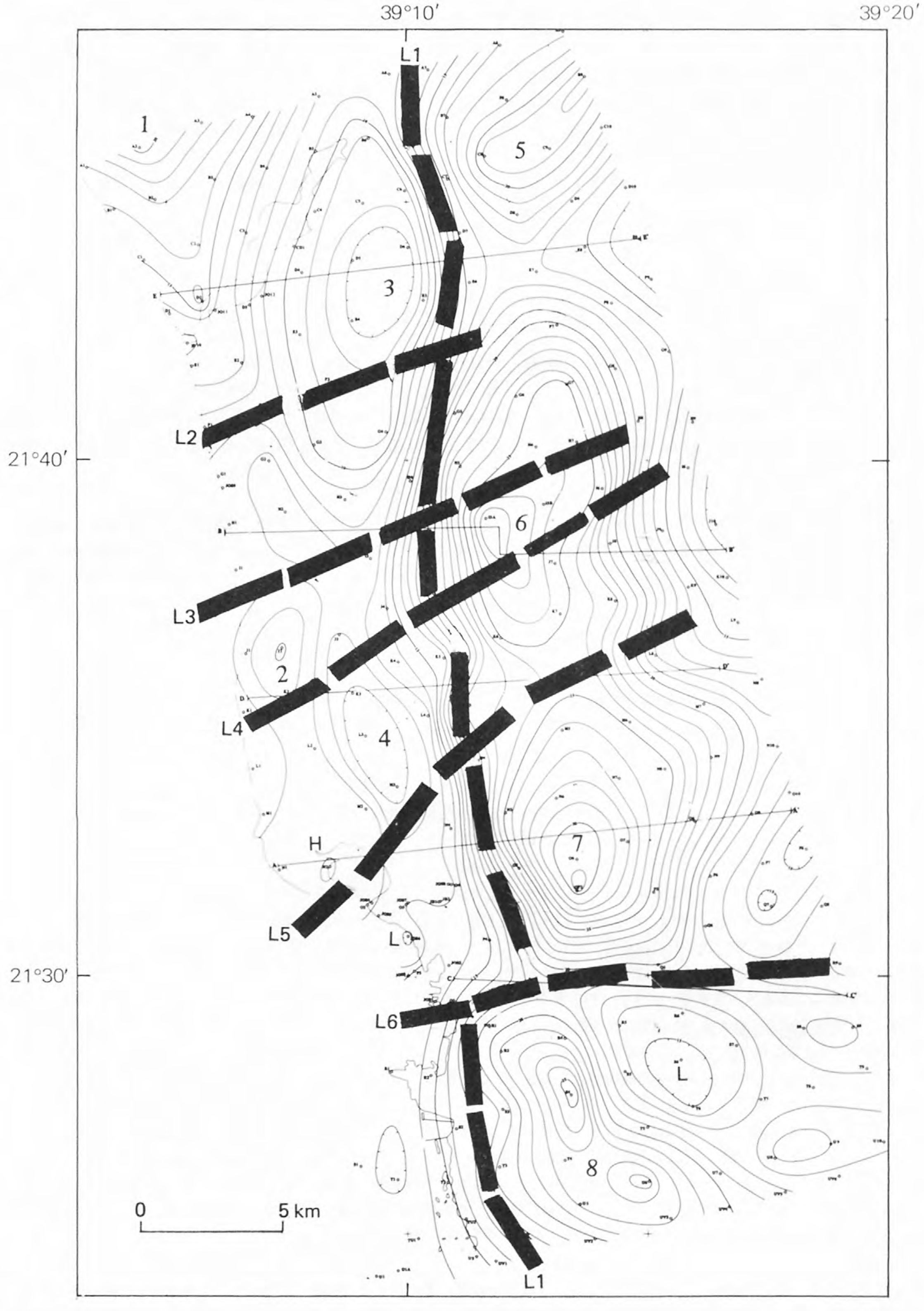

Figure 3.--Map showing the major features of the Bouguer gravity anomaly field of the Jiddah area. Discrete anomalies are labeled 1 to 8; major curvilinear (heavy dashed lines) features are labeled L1 to L5. H indicates relative high in the gravity field; L indicates relative low. Contour interval, 1 mgal. See text for detailed discussion and plate 1 for contour values.

which has a Bouguer gravity anomaly level of approximately 12 mgals, from Precambrian bedrock outcrops to the east, which have gravity levels of approximately 15 mgals. If we assume an average density contrast of 0.3 $g\text{-}cm^{-3}$ between the coastal plain sedimentary rocks and the Precambrian rocks, then calculation of a simple Bouguer slab model yields 250 m as the minimum thickness of sediments overlying basement. A larger density contrast would lead to smaller thickness estimates.

Apparent offsets of anomalies (for example, those labeled 3 and 6) were used to define five northeast- to east-trending curvilinear features on figure 3. Both offsets in the trends of anomalies (for example, between anomalies 3 and 4 and anomalies 7 and 8, fig. 3) and saddle points in anomalies of a linear nature were also used to define these features. Additionally, abrupt anomaly terminations, such as at the northern end of anomaly 8 and at the southern end of anomaly 7, helped define these features. These curvilinear features define boundaries of blocks that are systematically offset in a right-lateral sense, and we interpret them to be the gravity expression of strike-slip faults.

Although not obvious from the gravity anomaly map (plate 1) because of its limited east-west coverage, the map area lies in a region in which the Bouguer gravity anomaly field decreases to the east at a rate of from 1.1 to 1.25 $mgal\text{-}km^{-1}$ (Gettings, unpublished data, 1982). At the station spacing of the regional data (5-10 km), this gradient is essentially constant across the map area; it represents the change in the anomalous gravity field from positive values representative of the oceanic crust of the Red Sea (Allan, 1970) to negative values representative of the continental crust of the Arabian Shield. If this gradient is removed from east-west profiles across the map (see below), a much larger gravity anomaly between the sediments of the coastal plain and the Precambrian basement results. We will now show that such a regional gravity gradient is in good agreement with existing geologic and aeromagnetic data.

Aeromagnetic survey data offshore from Jiddah and both offshore and on the coastal plain to the north and south of Jiddah have been interpreted to approximate the depth to magnetic basement (Arabian Geophysical and Surveying Company, 1976a, sheet 14). From near the Precambrian outcrops westward to about halfway across the coastal plain, depth estimates are between 300 and 500 m; westward beyond this point, the depth estimates increase uniformly to a maximum depth of about 2 km at a distance of about 5 km offshore in the northern part of the map area.

Data from the two deepest drill holes in the area, one at lat 21°38.7' N., long 39°09.0' E. (Meissner, 1970), and the other at lat 21°27.2' N., long 39°11.4' E. (Skipwith, 1973), indicate that the magnetic basement at the two localities must be below depths of 500 m and 267 m, respectively. The drill-hole locations are shown on plate 3. Both of these holes intersected sedimentary sequences that contain interbedded evaporites. The drill-hole data and aeromagnetic interpretations suggest the simple model illustrated in figure 4.

In this model, we define the density contrast between the Precambrian rocks and the upper (sedimentary) layer to be $\Delta\rho_1$ and that between the Precambrian rocks and the lower layer to be $\Delta\rho_2$. Based on the results of the seismic deep-refraction line on the Tihamat Asir (Blank and others, 1979), we assume a crustal thickness of 15 km. For this model, composed of bodies 1 and 2, the gravity effect at each observation point is

$$\Delta g(x) = \Delta\rho_2 G_2 + \Delta\rho_1 G_1 \qquad (1)$$

where G_1 and G_2 are geometric factors dependent only on the shape and location of body 1 and body 2, respectively. The gravity gradient for a profile of equally spaced points is then given by

$$\frac{\Delta g_i - \Delta g_{i-1}}{h} = \frac{\Delta\rho_2 (G_{2,i} - G_{2,i-1})}{h} + \frac{\Delta\rho_1 (G_{1,i} - G_{1,i-1})}{h} \qquad (2)$$

where h is the station spacing and the subscript notation i and i-1 denotes the i^{th} point and the point immediately preceding it, respectively. If we now consider the expression $(G_{2,i} - G_{2,i-1})$ to be the dependent variable y and the expression $(G_{1,i} - G_{1,i-1})$ to be the independent variable x and denote the constant gradient $(\Delta g_i - \Delta g_{i-1})$ by g, we can rewrite equation (2) in the form

$$y = \frac{gh}{\Delta\rho_2} + \left(\frac{\Delta\rho_1}{\Delta\rho_2}\right)x \qquad (3)$$

This equation can be treated by linear regression methods and $\Delta\rho_1$ and $\Delta\rho_2$ determined in a least-squares sense. If h is 2 km and g is 1.1 mgal-km^{-1} and the sets of geometric factors $\{(G_{1,i})\}$ and $\{(G_{2,i})\}$ are computed from the expression for a two-dimensional body of polygonal cross section of unit density (Grant and West, 1965, p. 289), then a least-squares fit for a range of x across the map area yields for $\Delta\rho_1$ a value of -0.246 g-cm^{-3} and for $\Delta\rho_2$ a value of 0.030 g-cm^{-3}. The resulting gravity effect of the model is shown in figure 4. If a sampling interval of 5 km is used (fig. 4), the model yields an essentially constant gradient

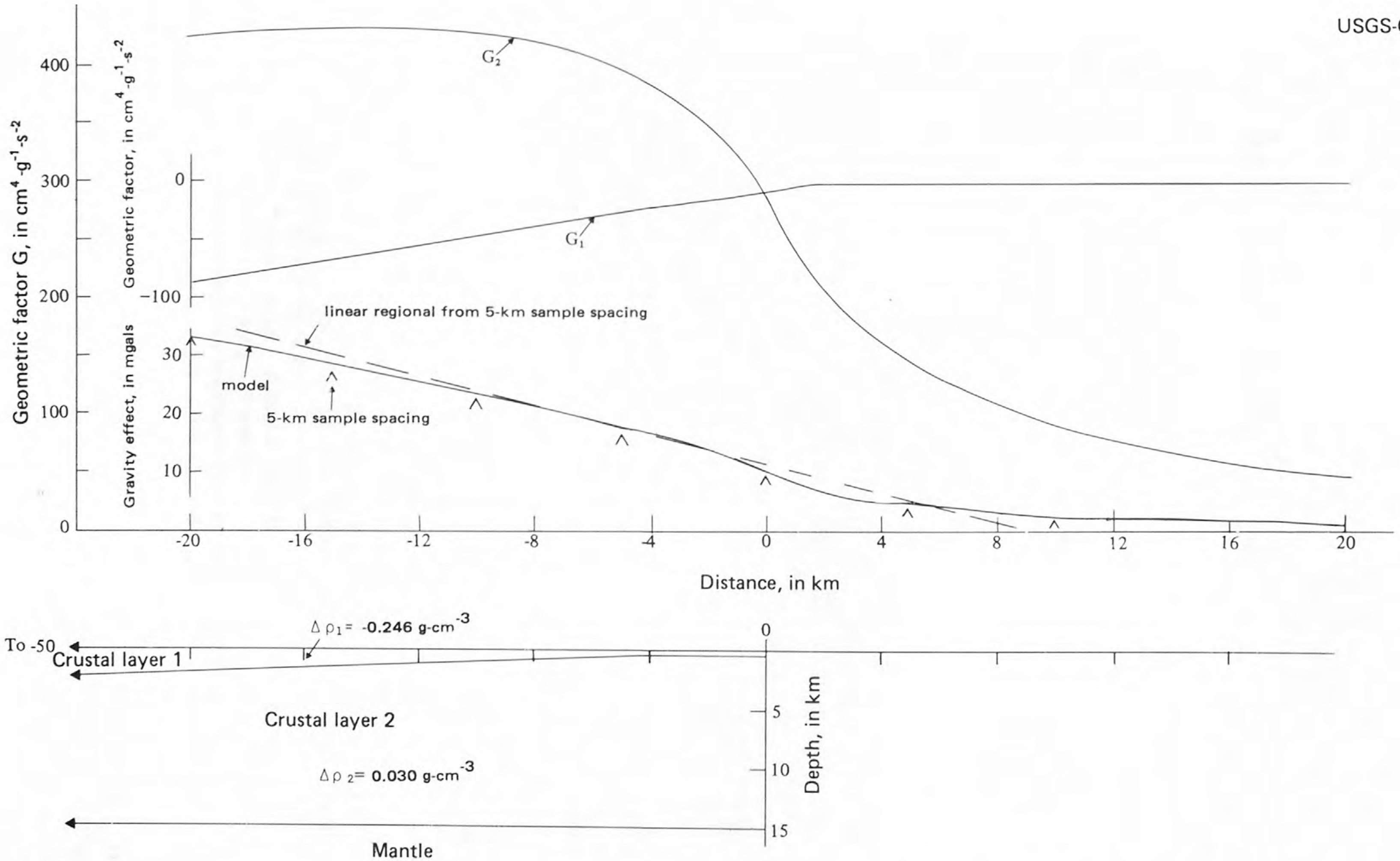

Figure 4.--Graphs showing cross section and gravity effect of a simple model that could explain the near-constant (5-km sample spacing) regional gravity gradient of approximately 1.1 mgal-km^{-1} decreasing to the east across the map area. The model geometry is based on drill-hole data and interpretation of aeromagnetic data; the density contrasts are then determined in a least-squares sense. The actual value of the gradient varies $\pm$10 percent, depending on where the samples are located. See text for details.

and thus satisfies the observations. The computed density contrast for layer 1 gives a quite reasonable average density of 2.4 g-cm^{-3} for the sedimentary rocks, and the computed density contrast for layer 2 is small and positive, which yields a density appropriate either for oceanic or continental crust. This simple crustal model, composed of a seaward-thickening wedge of marine sedimentary rocks overlying a basement of either downfaulted continental or oceanic crust, satisfies the constraints imposed by the existing geologic and geophysical data.

Aeromagnetic map of the Jiddah area

To facilitate interpretation of the gravity data, a map of the aeromagnetic field (plate 2) of the Jiddah area was compiled from all available data in the map area. Fortuitously, because a mean terrain clearance of 300 m was used in the collection of all data, no analytic field continuation was necessary in the compilation. For the area of Arabian Shield outcrop, sheets 21EE and 22EE at 1:50,000 scale were used; these were compiled for the Directorate General of Mineral Resources in 1965-1966 by a consortium headed by Aero Service Corporation Limited, under the supervision of Bureau de Recherches Geologiques et Minieres. These sheets were combined with sheet 22 of the aeromagnetic survey of the Saudi Arabia coastal areas flown for USGS in 1976 by the Arabian Geophysical and Surveying Company (ARGAS), as part of a survey done for the Saudi-Sudanese Red Sea Commission, and with those parts of the eight east-west Red Sea profiles, flown in 1969 by ARGAS, that are in the map area (Kabbani, 1970). Flight lines were northeast-southwest for both the Shield and coastal-plain surveys, and they had a mean spacing of 800 m on the Shield survey and 2,500 m on the coastal-plain survey. The magnetic field values on plate 2 are relative to an arbitrary datum.

The major features of the aeromagnetic map are shown on figure 5. We recognize that the definition of curvilinear features or trends is in part subjective, and we do not show every feature definable by the criteria listed above (anomaly offset, saddle points, continuity of gradients, and abrupt anomaly terminations). Moreover, we show only those curvilinear features that have considerable horizontal extent, that is, generally only those features that extend across the map area. The major trend directions are northeast and northwest. Anomaly 1 is the southern part of the "plug" anomaly referred to above, which probably represents a shallow intrusion located just north of the map area (see ARGAS, 1976a).

A dotted line delineates the approximate boundary between the very smooth magnetic field over the coastal plain and the

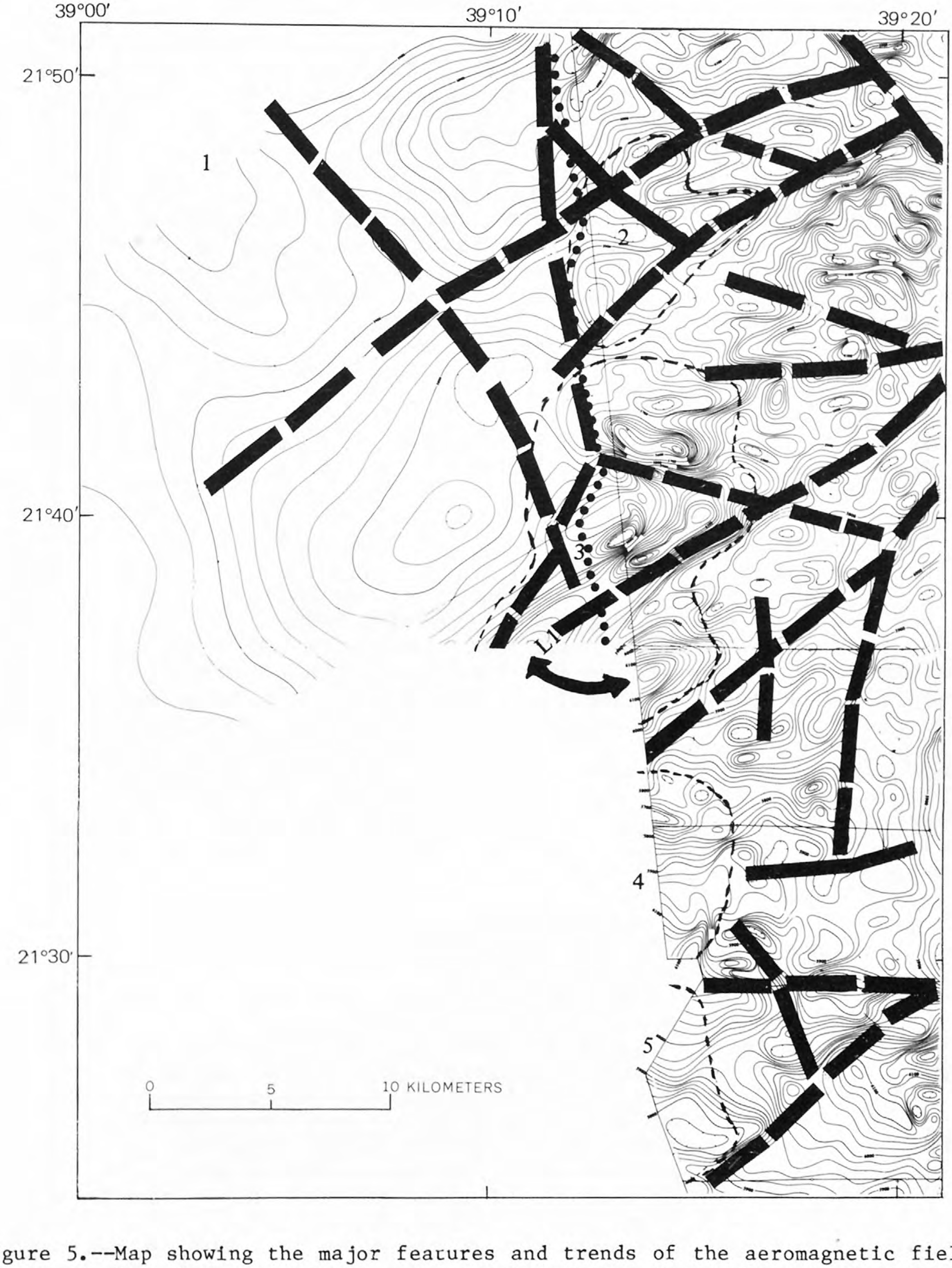

Figure 5.--Map showing the major features and trends of the aeromagnetic field map. Heavy dashed lines represent curvilinear features (one of which is labeled L1); thin dashed lines indicate boundaries of areas (numbered 2 through 5) of magnetic response that may be associated with corresponding positive gravity anomalies (fig. 2); dotted line represents the boundary between the magnetic field over the coastal plain (west) and that over the Precambrian terrane (east). Contour interval, 20 nT. See text for a detailed discussion.

much more varied field to the east over the Precambrian terrane. The thin dashed boundaries labeled from 2 through 5 indicate those areas of magnetic response that may be associated with the corresponding positive gravity anomalies of figure 3, which were interpreted to result from shallow mafic intrusions. Note on figure 5 that anomaly 5 is apparently reversely polarized and that anomalies 2 through 4 appear to be normally polarized. The boundaries of the anomalies were drawn based on a polarization either parallel or antiparallel with the Earth's field and after a study of the magnetic signatures of prismatic bodies at this magnetic latitude (see, for example, Andreasen and Zietz, 1969).

The stronger curvilinear features are shown as heavy dashed lines on figure 5; the feature labeled L1 is the most prominent curvilinear feature on the map, and its strike extension offshore (see ARGAS, 1976a, sheet 14) offsets an apparent sea-floor anomaly in a right-lateral sense.

The southern half of the map seems to be less dominated by northeast and northwest trends and exhibits more features trending east and north; however, this difference may be due to the less extensive map coverage in the south. Finally, we note that because of the lack of adequate data in the southwestern quadrant of anomaly 3, the magnetic high at the southwestern edge of the data aligned with lineament L1 may actually be part of the high located to the east-southeast and thus part of a normally polarized anomaly associated with a pluglike intrusive body. This uncertainty is indicated with a double-ended arrow on figure 5. From the available data, anomalies 2 through 5 are consistent with what would be expected from intrusive masses; however, all except anomaly 4 seem to be broken and offset by faults that have a significant strike-slip component.

Paleomagnetic results

In an effort to determine if the rocks causing the positive gravity anomalies were exposed, two field trips were taken to the outcrops that extend well into gravity anomaly 6 (fig. 3, plate 3), and paleomagnetic determinations were carried out on five oriented specimens in the USGS paleomagnetic laboratory in Jiddah. Alternating-field demagnetization was used to magnetically clean the samples, and measurements were made at cleaning levels of 0, 100, 200, 300, 400 and 600 oersted (Oe). The results of these measurements are shown in figure 6. Lithology and field relations for these specimens are summarized in table 1. Mean directions, computed by standard methods, are shown in table 2 for each cleaning level.

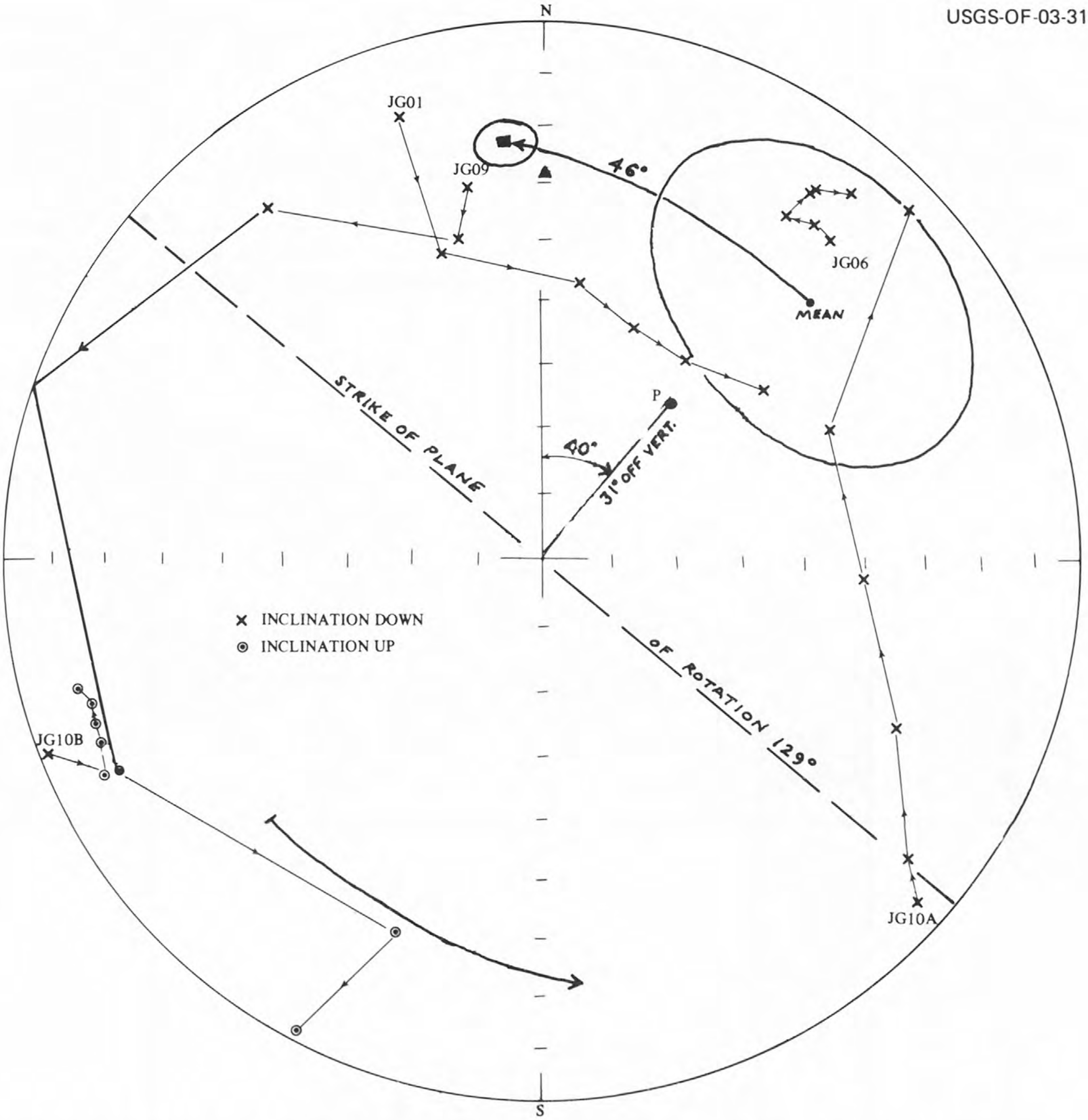

Figure 6.--Equal-area projection showing results of remanent magnetization measurements for five samples in the area of gravity anomaly 6 (see plate 3 for sample locations). Sample number is next to symbol showing direction of natural remanent magnetization vector. Subsequent symbols for each path show measured directions after alternating-field demagnetization steps. Point labeled "mean" represents the mean direction for the five samples (declination 46.6°, inclination 30.8°) at the 400-Oe demagnetization level. Square represents the pole position of the Tertiary As Sirat lavas (Kellogg and Reynolds, 1980), corrected for the latitude of the Jiddah area; triangle marks the present-day geomagnetic pole position. Ovals of 95 percent confidence limits are shown for both the mean and As Sirat pole positions. Point labeled "P" is the position of a pole of rotation that rotates the mean to the As Sirat pole in a simple rotation of 46°; the strike of the plane containing this rotation is also shown.

Table 1.--Lithology, field relations, bulk density, and magnetic susceptibility of five specimens collected in the greater Jiddah area

[Specimen localities shown on plate 3]

Specimen	Lithology	Bulk magnetic susceptibility (1E-6 cgs-cm^{-3})	Bulk density (g-cm^{-3})	Remarks
JG01	Granite	236	2.61	Deuterically altered, vuggy hypabyssal; JG01 and JG06 are part of granite that intrudes dacite-rhyolite flow sequence of JG10B
JG06	Granite	197	2.56	Deuterically altered, vuggy, hypabyssal; JG01 and JG06 are part of granite that intrudes dacite-rhyolite flow sequence of JG10B. Pervasive shearing at this locality
JG09	Felsite dike	297	2.62	Dike, in JG01-JG06 granite
JG10A	Basalt dike	1,071	2.86	Cuts flow sequence of JG10B, trends 110°, vertical dip
JG10B	Dacite flow	434	2.67	Sequence of steeply dipping dacite and rhyolite flows and breccias (probably exogenous dome); contains inclusions of granite identical to JG01 and JG06 in hand specimen, probably penecontemporaneous with granite

Table 2.--Results of remanent magnetization determinations for five specimens collected in the greater Jiddah area

[Demag level is the demagnetization field strength (in oersteds) used to magnetically clean the specimens. $\overline{D}$ is the mean declination, clockwise from true north; $\overline{I}$ is mean inclination, positive downwards. R is the sum of the 5 unit vectors; k is Fisher's (1953) best estimate of precision; α_{95} is the semiangle of the cone of 95 percent confidence. $\overline{D}$, $\overline{I}$, $\overline{R}$, and α_{95} in degrees. DM and DP are the semimajor and semiminor axes in degrees, respectively, of the oval of 95 percent confidence surrounding the paleomagnetic pole. In calculating the means, reversely polarized directions were reflected to the corresponding normally polarized directions]

Demag						Paleomagnetic pole			
level	$\overline{D}$	$\overline{I}$	R	k	α_{95}	Latitude	Longtitude	DM	DP
0	5.4	15.8	3.66	3.0	53.7	75.4° N.	162.6° W.	28.4	55.2
100	4.3	25.6	3.65	3.0	54.0	80.8° N.	168.0° W.	31.4	58.2
200	2.8	21.9	3.17	2.2	69.3	79.4° N.	155.9° W.	38.7	73.2
300	57.5	28.4	4.50	8.0	28.8	35.4° N.	125.6° E.	17.3	31.6
400	46.6	30.8	4.61	10.4	24.9	45.8° N.	127.4° E.	15.5	27.8
600	47.8	22.3	4.59	9.8	25.7	43.3° N.	133.7° E.	14.4	27.3

The results are least scattered at the 400-Oe cleaning level, and the best estimate of an average direction for normal polarity is a declination of 047° and an inclination of 31° for the two granite specimens and the mafic dike; the directions for both the dacite (JG10B) and felsite dike (JG09) are opposite to this direction (fig. 6). The average direction could represent either a geomagnetic pole direction or a tectonically rotated direction. If it represents the latter, then a possible rotation is shown in figure 6 that would bring the specimens to the mean normal and antinormal directions for the period from 29 to 24 Ma ago through a rotation of about 46°. This Oligocene-Miocene direction (corrected for the latitude of the study area) is defined by paleomagnetic studies of the lavas of the As Sirat volcanic field in southwestern Saudi Arabia (Kellogg and Reynolds, 1980) and is the most appropriate direction to use if the rotation is a result of Red Sea rift formation. As shown in figure 6, however, a rotation to the present-day pole would not be much different.

The rotation pole is 31° off vertical along a declination of 040° with a rotation of 46°; it is, however, subject to considerable error because of the large uncertainty (α_{95} = 25°) in the mean paleomagnetic direction. The field relations (table 1) imply that the granite and the dacite flow sequence are penecontemporaneous, but the dikes in each unit are of reverse polarity from their host rocks; thus the entire episode must have spanned several geomagnetic field reversals. This problem can be resolved only by further sampling and paleomagnetic analyses to verify the magnetization directions; here we simply note that the described rotation has the correct sense for a rotated block in a right-lateral strike-slip fault zone. Although such faulting is suggested by the aeromagnetic and Bouguer gravity anomaly data and geologic mapping, a rotation from the inferred intrusion in this area or a different geomagnetic field direction could produce the observed results and cannot be ruled out without further work.

Discussion of the geological and geophysical data

Plate 3 presents the generalized geologic relations in the map area, which are taken for the most part from Morris (1975). Supporting geologic information may be found in Brown and others (1963), Al-Shanti (1966), Brown (1970), Laurent and others (1973), Skipwith (1973), Nebert and others (1974), Hirayama (1977), Khallaf and others (1980), and Skiba (1980).

Precambrian rocks cropping out in the eastern half of the map area are predominantly diorite, granodiorite, and quartz diorite, with some granite and small areas of greenschistfacies layered rocks including some andesite flow rocks. Foliation and schistosity in these rocks generally trend northeast. All of these rocks have been regionally folded and are now exposed in broad, open folds that plunge approximately 20° NE. (Nebert and others, 1974). Half-wavelengths of the folds range from 0.5 to 1.0 km. Smaller scale folding is also present in varying degrees. At least three sets of normal faults are present; most faults are Tertiary in age or at least have had Tertiary movement (Al-Shanti, 1966; Nebert and others, 1974). The oldest set of Tertiary faults trends from 150° to 180°, and the two younger sets trend mainly northeast-southwest and northwest-southeast. Most of the faults are strongly curvilinear, particularly those of the northeast-trending set, many of which curve to more northerly trends along the fault trace to the northeast. Many of the fault displacements measured by Al-Shanti (1966) have a horizontal-to-vertical movement ratio of approximately 3:1, with both right- and left-lateral senses of motion for the strike-slip component. Extensive right-lateral strike-slip faulting is not directly proven in the detailed surface geologic mapping (Al-Shanti, 1966; Nebert and others, 1974); however, neither is it obviated. Moreover, the regional mapping of Khallaf and others (1980) strongly suggests such faulting, particularly along feature L1 of figure 5. Regional offset in a right-lateral sense for the entire Jiddah-Makkah area is also suggested by Blank (1977) from studies of aeromagnetic lineations.

The remainder of the map area is underlain mostly by unconsolidated sediments and alluvial material and includes a large area of coral limestone that forms a belt, approximately 5 km wide, along the coast north of Jiddah. A thin tongue of Quaternary basalt crops out in the northern part of the area.

Comparison of the geologic map (plate 3) with the aeromagnetic map (plate 2) results in the following observations. On the Precambrian outcrops, away from positive gravity anomalies 5 to 8 (fig. 3), magnetic anomalies tend to range in amplitude from 100 to 200 nT and have half-wavelengths of about 2 km or greater. The northeast-trending belt of quartz diorite near the center of the map area seems to have an identifiable magnetic anomaly associated with it; however, correlations with other map units are not as clear. Those units mapped as diorite and granite generally are associated with areas of low magnetic intensity, whereas those units mapped as granodiorite, quartz diorite, and andesite are generally in areas of higher magnetic intensity. The fact that these relations become more obscure in the areas of the gravity anomalies suggests that a separate, more intense anomaly from another source is masking the response of the exposed rocks. At least one east-northeast-trending magnetic anomaly follows the outline of a wadi; this suggests that a negative-weathering, more magnetic unit may form the bedrock of the wadi. The anomaly is at a bulge of the northeastern flank of gravity anomaly 7 and thus could be a large mafic dike.

The reasonably good correlation between the trends and offsets in magnetic anomalies and gradients on plate 2 and the mapped faults and contacts on plate 3 suggests that more faulting and fracturing may be present than has been mapped by Morris (1975). Khallaf and others (1980) also suggested more faulting, particularly faulting trending northeast, in their map. We note that in this magnetic latitude north-trending boundaries of blocks having different magnetic properties will fall beneath gradients in the magnetic field, whereas east-west boundaries will fall near the anomaly maxima and minima (see Andreasen and Zietz, 1969).

The trends and anomalies (plate 2) in the coastal-plain areas do not correlate with any of the map units but instead are parallel with anomalies in the Red Sea interpreted as sea-floor magnetic anomalies and extensions of transform faults (ARGAS, 1976a; Hall, 1979). The computed depths to magnetic basement (ARGAS, 1976a) of these anomalies are approximately 1 km below sea level near the coastline (see plate 3), and, although the best test of the nature of the magnetic basement beneath the coastal plain would be to upward continue to a height of 1 km the aeromagnetic data over the Precambrian rocks east of the coastal plain, at least some insight can be gained by study of an example in an area in which the continuation has already been done. The Harrat Rahat aeromagnetic survey (ARGAS, 1976b) contained as part of its specifications not only residual-field maps but also upward-continuation maps analytically upward continued by 1 km. Because the terrain clearance and flight-line spacing of the two surveys are identical, if one chooses magnetic anomalies on the Harrat Rahat residual maps having similar amplitudes and half-wavelengths to those observed over the Precambrian outcrops in the Jiddah area and then inspects the resulting upward-continued anomalies, a feeling can be gained as to how the anomalies of the Jiddah area should look at a depth of 1 km. The results of this exercise suggest that the magnetic anomalies in the Jiddah area should be more intricate, contain more anomalies of shorter wavelength (half-wavelengths of from 3 to 5 km), and probably be of larger amplitude than outlined by this survey. These disparities imply either that the depth estimates are considerably in error and the Precambrian basement is much deeper than suspected or that there is a change in the character of the magnetic crust between Precambrian crust and either oceanic crust or Precambrian crust having different magnetic properties and spatial distribution.

A comparison of the Bouguer gravity anomaly map (plate 1) to the geologic map (plate 3) in the areas of Precambrian exposure shows that at this station spacing and contour interval the gravity field is not much perturbed by the mapped lithologic changes. The one exception to this observation is the quartz diorite unit in the central part of plate 3, which seems to have a systematically lower bulk density than other units of the Precambrian terrane. As mentioned above, the belt of low-amplitude gravity anomaly highs along the coastline and the associated lows immediately east of them probably represent the change from interfingering marine sediments and clastic alluvial material of Precambrian outcrops to the east to a predominantly marine sedimentary section near the coastline (see Morris, 1975, p. 24). Because no terrain corrections have been applied to account for the seawater, the gravity anomaly values should decrease at the coastline, a decrease that would produce a linear high along the coast.

The gravity anomaly map (plate 1) and aeromagnetic map (plate 2) compare favorably and complement each other in that both define some anomalous areas not present on the other. The interpreted boundaries between areas having differing densities or magnetizations are shown on plate 3. Because of the lack of gravity survey coverage farther to the east and the uncertainty in anomaly definition due to the gradient L1 (fig. 3), the boundaries of the gabbroic intrusive bodies, as inferred from the gravity data (plate 3), have been conservatively chosen. This procedure results in minimum estimates for the causative sources of gravity anomalies 5, 6, 7, and 8 (fig. 3), such that they are systematically smaller in plan than the corresponding boundaries as inferred from the aeromagnetic data (see plate 3). The inferred source of magnetic anomaly 4 (fig. 5) is displaced southward from the inferred source of gravity anomaly 7 (fig. 3). Whether this is a real effect or an artifice cannot be evaluated without further aeromagnetic data to define the western half of the anomaly and refine the boundary of the eastern half. Some of the curvilinear gravity features shown on plate 3 are displaced about a kilometer to the north of the corresponding magnetic feature. Although this displacement partly results from not knowing precisely where to draw the features on the basis of the gravity data, it mostly results from attempting to draw these curvilinear features on the basis the aeromagnetic data because of the complexity introduced by overlap of neighboring anomalies.

Finally, we note the analogy between the aeromagnetic and gravity fields in the Jiddah area and those near Precambrian outcrops in the Tihamat Asir to the south (Gettings, 1977). In the Tihamat Asir, similar discrete gravity anomalies of about the same half-wavelength and amplitude have been observed near the edge of Precambrian outcrops and result from exposed Tertiary layered gabbro intrusive bodies located at the suture zone between Precambrian continental and Tertiary oceanic crust.

The above evidence suggests that the continental margin is located at or near gravity anomaly gradient L1 (fig. 3), with oceanic crust to the west beneath the coastal plain and Precambrian continental crust to the east; we propose that the large, positive gravity anomalies numbered from 5 to 8 (fig. 3) represent shallow mafic intrusive bodies, probably of Tertiary age, located along this boundary zone. A diagrammatic representation of this model is shown in figure 7.

In figure 8, a series of profiles (see plate 1 for profile locations) are shown both with and without the removal of an eastward-decreasing regional gradient of 1.1 mgal-km^{-1}. Because the bulk density of the upper few kilometers of oceanic crust is quite similar to that of the Precambrian shield (Worzel, 1974) and because the map coverage is insufficient to define the anomalous field for deeper sources, we restrict our interpretation to an estimation of the thickness of the marine sedimentary rocks and a derivation of minimum limits on the geometry of the hypothesized mafic intrusive bodies. Profiles D-D' and E-E' (fig. 8) suggest a steeply dipping step or interface between the sedimentary and crystalline rocks. Because of the superposition of gravity anomaly highs 6 through 8 on this gradient, any information on the dip of the interface contained in the gravity anomaly field is obscured. We observe, however, that as the distance from the interface increases the gravity effect of a step approaches that of a Bouguer slab. Using profiles A-A', B-B', D-D', and E-E' (fig. 8), we infer that the gravity effect must range from 15 to 21 mgal.

The available drill-hole information (Meissner, 1970; Skipwith, 1973) suggests that the sediments are at least 500 m thick at lat 21°38.7' N., long 39°09.0' E., and 270 m thick at lat 21°27.2' N., long 39°11.4 E. Using data from the logs of these holes and published density measurements (Daly and others, 1966), we infer that the average density of the sedimentary section probably ranges from 2.35 to 2.45 g-cm^{-3}. Because the average value for the density of the Precambrian rocks probably ranges from 2.65 to 2.75 g-cm^{-3}, the mean density contrast between the two units probably ranges from 0.25 to 0.35 g-cm^{-3}. For a slab model, such a density contrast gives a thickness of approximately 1.5 km for a gravity anomaly of from 15 to 21 mgal. Because the effect of the positive anomalies is to increase the anomalous gravity field and because of the lack of coverage well to the east of these anomalies, this value should be considered an upper bound on the thickness estimate. In this simple model, no account has

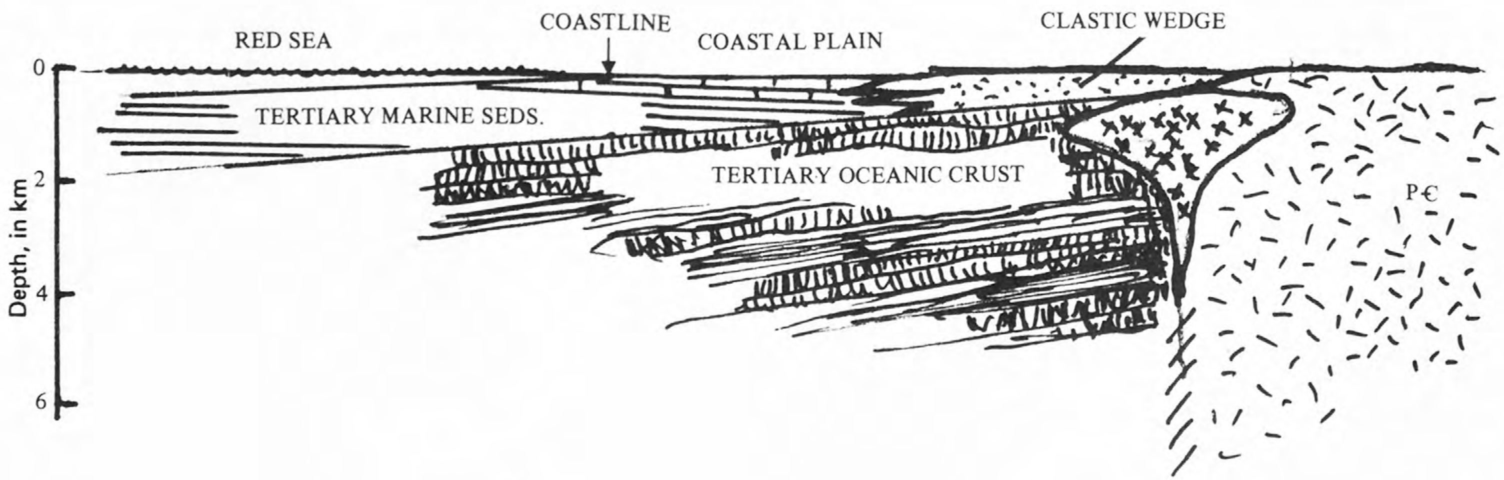

Figure 7.--Diagrammatic cross section showing the interpretational model adopted, which qualitatively fits existing geologic and geophysical data in the Jiddah area. Although the boundary between the oceanic and continental crust probably dips steeply, there is no strong evidence to indicate if the dip is east or west; thus it is taken as vertical.

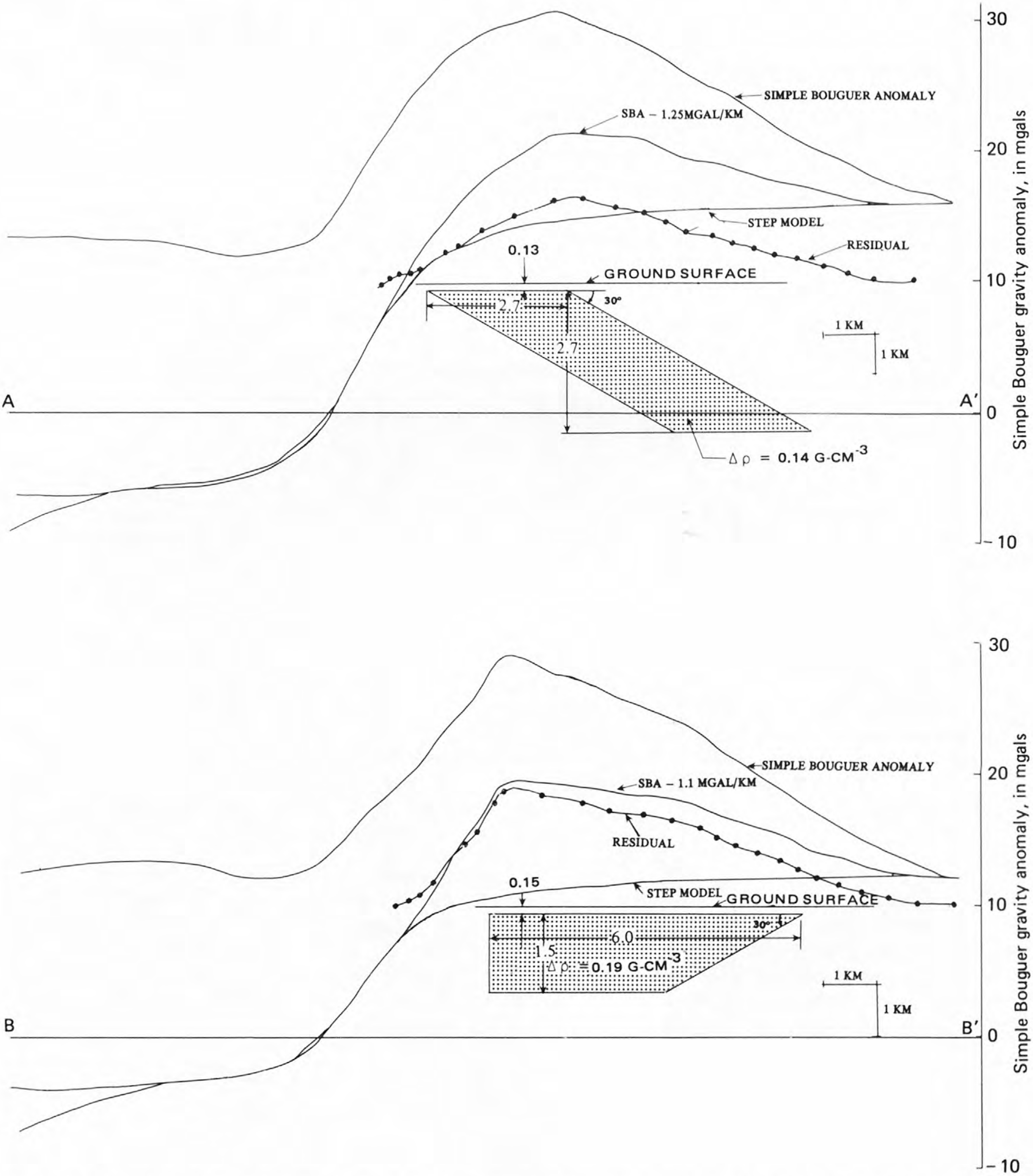

Figure 8.--Graphs showing the simple Bouguer gravity anomaly field (see plate 1 for profile locations) and the resulting residual profiles after subtraction of an eastward-decreasing regional gradient of 1.1 mgal-km^{-1} (1.25 for A-A'). For profiles A-A' and B-B', the step model shown has been removed from the simple Bouguer anomaly to give a minimum residual anomaly attributed to a mafic intrusion. Interpretation by curve matching to an album of two-dimensional model curves (Phoenix Corporation, 1980) yields the geometric shapes and density contrasts illustrated as the best fits.

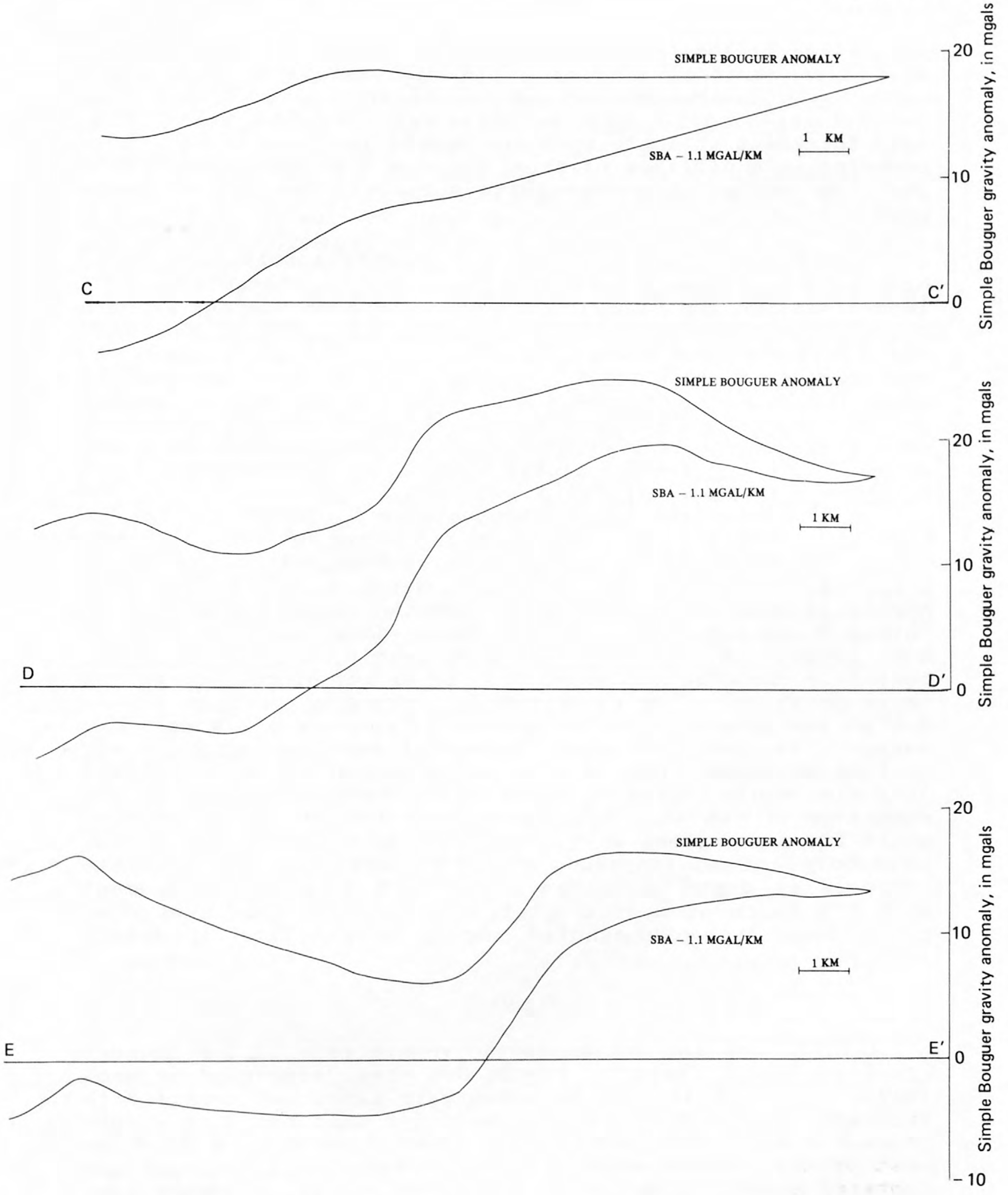

Figure 8.--Continued

been taken of the probable thickening of the sediments to the west (see regional gravity field discussion, above); moreover, only the asymptotic values of the anomaly have been used in this model. Despite these factors, the agreement of this thickness estimate with the depths to magnetic basement, computed at a distance of from 1.0 to 1.5 km immediately offshore by using the aeromagnetic survey (plate 3), is quite good.

Interpreted cross sections for gravity anomalies 6 and 7 are shown in figure 8 (profiles A-A', B-B'). These show minimum limits on the size of the intrusive body because in both cases a vertical-interface step model was used that brings the residual anomaly to zero at both the "knee" on the west side of the anomaly and to the limits of the data on the east side. The residual anomaly attributed to the intrusive body is thus minimized. The resulting residual gravity anomalies were then appropriately plotted and curve matched to model curves for a two-dimensional model of trapezoidal cross section (Phoenix Corporation, 1980). The use of a two-dimensional rather than a three-dimensional model tends to underrepresent both the size and the depth of the causative body. The cross sections yielding the best fits are shown in figure 8. Note that the estimated depth to the top of both models is approximately 150 m, and the density contrast is betwen 0.15 and 0.20 $g\text{-}cm^{-3}$; these data imply a minimum bulk density of from 2.85 to 2.90 $g\text{-}cm^{-3}$, and we therefore postulate that the intrusive body is either diorite or gabbro in composition. The interpreted thicknesses of from 1.5 to 3.0 km are also typical of gabbro intrusions of laccolithic shape. If the step model that defines the residual was shifted eastward, then the westward extent of the inferred intrusion would increase, as would the inferred mass. If the magnitude of the step was decreased, then the inferred mass would increase; these shifts would produce both a more extensive body and an increased density contrast. The probable increase in depth estimates might lead to better agreement with the depth of approximately 400 m below sea level computed from the aeromagnetic survey data (plate 3; ARGAS, 1976a).

SUMMARY

Qualitative and semiquantitative analysis of the Bouguer gravity anomaly field in the Jiddah area, supported by geologic, aeromagnetic, and paleomagnetic data, has resulted in two major hypotheses. First, we infer that the suture zone between oceanic and continental crust lies from 3 to 5 km west of the western edge of exposed Precambrian outcrops and contains several large mafic intrusive bodies, probably gabbroic in composition. Second, we infer that the area contains extensive northeast-trending faults that have a signif-

icant strike-slip component, mostly of a right-lateral sense. These faults seem to trend some distance into the Precambrian rocks and overlying Tertiary rocks to the east (Lambolez and Pilet, 1968), a relationship which suggests that much of the faulting in the Jiddah area is of Tertiary age and associated with Red Sea rifting. Much of the faulting may represent Tertiary reactivation of preexisting faults and fractures. The interpreted extent of the major structures inferred from gravity and aeromagnetic data is shown on plate 3.

Preliminary paleomagnetic results suggest that detailed studies in the area might help delineate deformation caused by both intrusive activity and Red Sea-related faulting.

Further study of the nature of the crust beneath the coastal plain should be conducted; the first step might be upward-continuation studies of the aeromagnetic data on the Precambrian terrane north and south of Jiddah and a detailed comparison of this data with the coastal-plain and offshore data. Finally, the results of this work, as well as those from the monitoring of microseismic activity by Merghelani (oral commun., 1981), suggest that the offshore Red Sea transform fault zone (Hall, 1979) may extend inland in the Jiddah area and that a detailed study of this zone (USGS Saudi Arabian Mission, 1979, p. 19) could yield insight into the mechanism of transform faulting during rifting.

REFERENCES CITED

Al-Shanti, A. M. S., 1966, Oolitic iron ore deposits in Wadi Fatima between Jeddah and Mecca, Saudi Arabia: Saudi Arabian Directorate General of Mineral Resources Bulletin 2, 51 p.

Allan, T. D., 1970, Magnetic and gravity fields over the Red Sea: Philosophical Transactions of the Royal Society of London, v. 267A, p. 153-180.

Andreasen, G. E., and Zietz, Isidore, 1969, Magnetic fields for a 4 x 6 prismatic model: U.S. Geological Survey Professional Paper 666, 9 p.

Arabian Geophysical and Surveying Company, 1976a, Aeromagnetic survey, Saudi Arabia coastal plain areas: Arabian Geophysical and Surveying Company survey 201-0965, for the Saudi-Sudanese Red Sea Commission and U.S. Geological Survey, 19 p., 33 plates.

__________ 1976b, Airborne magnetometer survey, Harrat Rahat: Arabian Geophysical and Surveying Company survey 201-0969, for the Saudi Arabian Directorate General of Mineral Resources and U.S. Geological Survey-Bureau de Recherches Geologiques et Minieres, 22 p., 31 plates.

Blank, H. R., Jr., 1977, Aeromagnetic and geologic study of Tertiary dikes and related structures on the Arabian margin of the Red Sea, in Red Sea research 1970-1975: Saudi Arabian Directorate General of Mineral Resources Bulletin 22, p. G1-G18.

Blank, H. R., Healy, J. H., Roller, John, Lamson, Ralph, Fisher, Fred, McClearn, Robert, and Allen, Steve, 1979, Seismic refraction profile, Kingdom of Saudi Arabia-field operations, instrumentation, and initial results: U.S. Geological Survey Saudi Arabian Project Report 259, 49 p.

Blank, H. R., Jr., Henderson, J. R., Gettings, M. E., and Andreasen, G. E., 1980, Proposal for gravity and aeromagnetic /radiometric regional survey contract work, Kingdom of Saudi Arabia, program summary and work plan: U.S. Geological Survey Saudi Arabian Mission unpublished administrative document, available from U.S. Geological Survey, Jiddah, 11 p.

Brown, G. F., 1970, Eastern margin of the Red Sea and the coastal structures in Saudi Arabia: Philosophical Transactions of the Royal Society of London, v. 267A, p. 75-87.

Brown, G. F., Jackson, R. O., Bogue, R. G., and MacLean, W. H., 1963, Geologic map of the Southern Hijaz quadrangle, Kingdom of Saudia Arabia: U.S. Geological Survey Miscellaneous Geologic Investigations Map I-210 A, scale 1:500,000.

Daly, R. A., Manger, G. E., and Clark, S. P., Jr., 1966, Density of rocks, in Clark, S. P., Jr., ed., Handbook of physical constants: Geological Society of America Memoir 97, p. 19-26.

Donzeau, M. A. M., 1979, Program HP9004: Altimetric elevation calculation: U.S. Geological Survey Saudi Arabian Project Miscellaneous Document 7 (Interagency Report 285), 40 p.

Fisher, R. A., 1953, Dispersion on a sphere: Proceedings of the Royal Society of London, v. A217, p. 295-305.

Gettings, M. E., 1977, Delineation of the continental margin in the southern Red Sea region from new gravity evidence, in Red Sea research 1970-1975: Saudi Arabian Directorate General of Mineral Resources Bulletin 22, p. K1-K11.

__________ 1979, Program HP9001: Single base altimetry data reduction: U.S. Geological Survey Saudi Arabian Project Miscellaneous Document 3 (Interagency Report 281), 31 p.

Grant, F. S., and West, G. F., 1965, Interpretation theory in applied geophysics: New York, McGraw-Hill, 584 p.

Hall, S. A., 1979, A total intensity magnetic anomaly map of the Red Sea and its interpretation: U.S. Geological Survey Saudi Arabian Project Report 275, 260 p.

Hirayama, Jiro, 1977, Stratigraphy of the Fatima Formation: Saudi Arabian Directorate General of Mineral Resources Technical Record TR-1977-8, 8 p.

Kabbanni, F. K., 1970, Geophysical and structural aspects of the central Red Sea rift valley: Philosophical Transactions of the Royal Society of London, v. 267A, p. 89-97.

Kellogg, K. S., and Reynolds, R. L., 1980, Paleomagnetic study of the As Sarat volcanic field, southwestern Saudi Arabia: U.S. Geological Survey Saudi Arabian Mission Technical Record 14 (Interagency Report 360), 31 p.

Khallaf, H. M., Al-Khatieb, S. O., Skiba, W. J., and Zakir, F. M., 1980, The reconnaissance geologic map of the Jiddah north quadrangle, 21/39A; compiled by D. J. Grainger: Saudi Arabian Directorate General of Mineral Resources Open-File Report DGMR-753, scale 1:100,000.

Lambolez, B., and Pilet, P., 1968, Airborne magnetic sheet 136B preinterpretation: Bureau de Recherches Geologiques et Minieres (Saudi Arabian Mission) Report 68-JED-18, 6 p.

Laurent, D., Daessle, M., Berton, Y., and Dehlavi, M., 1973, Engineering geological map of Jiddah and spot information map on ground conditions in Jiddah, Kingdom of Saudi Arabia: Saudi Arabian Directorate General of Mineral Resources Geologic Map GM-8, scale 1:10,000.

Longman, I. M., 1959, Formulas for computing the tidal accelerations due to the moon and the sun: Journal of Geophysical Research, v. 64, p. 2351-2355.

Meissner, C. R., Jr., 1970, Notes on the significant results of a research study for possibilities of potash in Saudi Arabia: Unpublished memorandum to R. O. Jackson, available from U.S. Geological Survey Saudi Arabian Mission, Jiddah, 2 p.

Morris, P. G., 1975, Construction materials, non-metallic mineral occurrences, and engineering geology of the district around Jiddah, Kingdom of Saudi Arabia: Saudi Arabian Directorate General of Mineral Resources Technical Record TR-1975-1, 27 p.

Nebert, K., Alshaibi, A. A., Awlia, M., Bounny, I., Nawab, Z. A., Sharief, O. H., Sherbini, O. A., and Yeslam, A. H., 1974, Geology of the area north of Wadi Fatima, Kingdom of Saudi Arabia: Jiddah, King Abdulaziz University, Center for Applied Geology Bulletin 1, 31 p.

Phoenix Corporation, 1980, Total-intensity magnetic and gravity effects for 2D and 3D models at geomagnetic inclination 30°: Prepared by Phoenix Corporation, McLean, Virginia, U.S.A., for the U.S. Geological Survey and the Saudi Arabian Directorate General of Mineral Resources, 38 p.

Skiba, W. J., 1980, The form and evolution of late Precambrian plutonic masses in the Jiddah-Rabigh-Wadi Al-Quaha area, Saudi Arabia, in Evolution and mineralization of the Arabian-Nubian Shield: King Abdulaziz University, Institute of Applied Geology Bulletin 3, v. 3: Oxford-New York, Pergamon, p. 105-120.

Skipwith, Patrick, 1973, The Red Sea and coastal plain of the Kingdom of Saudi Arabia: Saudi Arabian Directorate General of Mineral Resources Technical Record TR-1973-1, 149 p.

U.S. Geological Survey Saudi Arabian Mission, 1979, Work plan of the USGS Mission for the fiscal year 1399: Unpublished administrative document available from U.S. Geological Survey Saudi Arabian Mission, Jiddah, Saudi Arabia, 37 p.

Worzel, J. L., 1974, Standard oceanic and continental structure, in Burk, C. A., and Drake, C. L., eds., The geology of continental margins: Berlin, Springer-Verlag, p. 59-66.

Appendix--*Principal facts for the 215 gravity stations used in the gravity survey of the greater Jiddah area*

[Bouguer gravity anomalies computed using a reduction density of 2.67 $g\text{-}cm^{-3}$ and relative to the 1930 Potsdam gravity datum. Heading abbreviations: ID, station identification; LAT, station latitude (in degrees, minutes); LONG, station longitude (in degrees, minutes); ELEV, station altitude (in m); OG, observed gravity (in mgals); THG, theoretical gravity calculated using the 1930 International Gravity Formula (in mgals); FAA, free-air gravity anomaly (in mgals); SBA, simple Bouger gravity anomaly (in mgals); HTC, inner-zone terrain correction (in mgals); TTC, total terrain correction (in mgals); CC, curvature correction (in mgals); CBA, complete Bouguer anomaly (in mgals); S.D. CBA, estimated standard deviation of CBA (in mgals). Terrain corrections were not computed for the stations in this survey]

Stations established with LaCoste-Ramberg gravimeter G330

ID	LAT	LONG	ELEV	OG	THG	FAA	SBA	HTC	TTC	CC	CBA	S.D.CBA	ID
JB1	21 31.310	39 10.550	5.0M	978753.58	978742.42	12.71	12.15	0.00	0.00	0.01	12.14	0.35	JB1
J001	21 29.360	39 10.400	0.0M	978754.14	978740.42	13.72	13.72	0.00	0.00	0.00	13.72	0.15	J001
J002	21 30.060	39 10.710	0.0M	978754.96	978741.14	13.82	13.82	0.00	0.00	0.00	13.82	0.15	J002
J003	21 29.880	39 9.850	0.0M	978754.12	978740.95	13.17	13.17	0.00	0.00	0.00	13.17	0.15	J003
JB1	21 31.310	39 10.550	5.0M	978753.58	978742.42	12.71	12.15	0.00	0.00	0.01	12.14	0.35	JB1
JB1	21 31.310	39 10.550	5.0M	978753.58	978742.42	12.71	12.15	0.00	0.00	0.01	12.14	0.35	JB1
J004	21 31.340	39 9.100	0.0M	978756.02	978742.45	13.57	13.57	0.00	0.00	0.00	13.57	0.15	J004
J005	21 31.080	39 9.230	0.0M	978754.89	978742.18	12.70	12.70	0.00	0.00	0.00	12.70	0.15	J005
J006	21 31.660	39 9.850	0.0M	978754.72	978742.78	11.94	11.94	0.00	0.00	0.00	11.94	0.15	J006
J007	21 31.330	39 9.860	3.0M	978754.82	978742.44	13.31	12.98	0.00	0.00	0.00	12.97	0.35	J007
J008	21 31.670	39 10.730	5.0M	978754.24	978742.79	13.00	12.44	0.00	0.00	0.01	12.43	0.35	J008
J009	21 39.630	39 6.060	0.0M	978763.05	978750.96	12.09	12.09	0.00	0.00	0.00	12.09	0.15	J009
J010	21 42.510	39 5.380	0.0M	978768.23	978753.92	14.31	14.31	0.00	0.00	0.00	14.31	0.15	J010
J011	21 43.140	39 5.970	0.0M	978768.27	978754.57	13.69	13.69	0.00	0.00	0.00	13.69	0.15	J011
J012	21 43.410	39 6.970	0.0M	978765.98	978754.85	11.13	11.13	0.00	0.00	0.00	11.13	0.15	J012
JB1	21 31.310	39 10.550	5.0M	978753.58	978742.42	12.71	12.15	0.00	0.00	0.01	12.14	0.35	JB1
JB1	21 31.310	39 10.550	5.0M	978753.58	978742.42	12.71	12.15	0.00	0.00	0.01	12.14	0.35	JB1
M1	21 33.130	39 6.800	0.0M	978757.11	978744.28	12.83	12.83	0.00	0.00	0.00	12.83	0.15	M1
M2	21 33.200	39 9.000	1.9M	978757.53	978744.35	13.76	13.55	0.00	0.00	0.00	13.54	0.32	M2
M3	21 33.630	39 9.670	7.2M	978753.94	978744.79	11.37	10.56	0.00	0.00	0.01	10.55	0.48	M3
M4	21 34.130	39 11.430	21.3M	978761.84	978745.31	23.11	20.73	0.00	0.00	0.03	20.69	0.67	M4
N5	21 33.090	39 11.950	19.5M	978766.10	978744.24	27.88	25.70	0.00	0.00	0.03	25.67	0.70	N5
N4	21 32.790	39 10.800	12.2M	978754.88	978743.93	14.72	13.35	0.00	0.00	0.02	13.33	0.41	N4
JB1	21 31.310	39 10.550	5.0M	978753.58	978742.42	12.71	12.15	0.00	0.00	0.01	12.14	0.38	JB1
JB2	21 31.330	39 10.580	7.6M	978753.44	978742.44	13.35	12.50	0.00	0.00	0.01	12.49	0.39	JB2
JB1	21 31.310	39 10.550	5.0M	978753.58	978742.42	12.71	12.15	0.00	0.00	0.01	12.14	0.35	JB1
N3	21 32.490	39 9.630	6.1M	978754.52	978743.63	12.77	12.09	0.00	0.00	0.01	12.08	0.35	N3
N2	21 32.080	39 8.200	0.0M	978757.32	978743.21	14.11	14.11	0.00	0.00	0.00	14.11	0.15	N2
M2	21 33.200	39 9.000	1.9M	978757.44	978744.35	13.68	13.47	0.00	0.00	0.00	13.46	0.35	M2
02	21 31.300	39 8.990	0.5M	978755.95	978742.41	13.69	13.64	0.00	0.00	0.00	13.64	0.15	02
03	21 31.290	39 9.820	3.1M	978754.83	978742.40	13.39	13.04	0.00	0.00	0.00	13.04	0.35	03

Appendix--*Principal facts for the 215 gravity stations used in the gravity survey of the greater Jiddah area*--Continued

ID	LAT	LONG	ELEV	OG	THG	FAA	SBA	HTC	TTC	CC	CBA	S.D.CBA	ID
JB1	21 31.310	39 10.550	5.0M	978753.58	978742.42	12.71	12.15	0.00	0.00	0.01	12.14	0.38	JB1
JB2	21 31.330	39 10.580	7.6M	978753.44	978742.44	13.35	12.50	0.00	0.00	0.01	12.49	0.35	JB2
JB2	21 31.330	39 10.580	7.6M	978753.44	978742.44	13.35	12.50	0.00	0.00	0.01	12.49	0.35	JB2
03	21 31.290	39 9.820	3.1M	978754.68	978742.40	13.24	12.90	0.00	0.00	0.00	12.89	0.35	03
04	21 31.680	39 10.760	6.5M	978754.18	978742.80	13.39	12.66	0.00	0.00	0.01	12.65	0.35	04
05	21 31.940	39 12.250	14.2M	978764.82	978743.06	26.15	24.56	0.00	0.00	0.02	24.54	0.35	05
06	21 32.130	39 13.460	28.7M	978768.16	978743.26	33.76	30.55	0.00	0.00	0.04	30.51	0.35	06
07	21 32.470	39 14.560	42.2M	978763.39	978743.61	32.81	28.09	0.00	0.00	0.06	28.03	0.35	07
P4	21 30.560	39 11.570	10.0M	978754.57	978741.65	16.01	14.89	0.00	0.00	0.01	14.88	0.58	P4
OP1	21 31.280	39 12.150	11.4M	978759.37	978742.39	20.50	19.23	0.00	0.00	0.02	19.21	0.42	OP1
OP2	21 31.500	39 13.470	26.2M	978768.43	978742.61	33.91	30.98	0.00	0.00	0.04	30.94	0.35	OP2
05	21 31.940	39 12.250	14.2M	978764.82	978743.06	26.14	24.55	0.00	0.00	0.02	24.53	0.35	05
JB2	21 31.330	39 10.580	7.6M	978753.44	978742.44	13.35	12.50	0.00	0.00	0.01	12.49	0.21	JB2
JB2	21 31.330	39 10.580	7.6M	978753.44	978742.44	13.35	12.50	0.00	0.00	0.01	12.49	0.23	JB2
P3	21 29.970	39 9.970	0.3M	978754.13	978741.05	13.18	13.14	0.00	0.00	0.00	13.14	0.13	P3
Q2	21 29.320	39 10.680	0.5M	978754.73	978740.38	14.50	14.45	0.00	0.00	0.00	14.45	0.13	Q2
Q3	21 29.640	39 12.270	11.9M	978755.89	978740.71	18.86	17.53	0.00	0.00	0.02	17.51	0.35	Q3
N1	21 32.030	39 7.130	0.0M	978756.80	978743.15	13.64	13.64	0.00	0.00	0.00	13.64	0.13	N1
JB2	21 31.330	39 10.580	7.6M	978753.44	978742.44	13.35	12.50	0.00	0.00	0.01	12.49	0.21	JB2
JB2	21 31.330	39 10.580	7.6M	978753.44	978742.44	13.35	12.50	0.00	0.00	0.01	12.49	0.21	JB2
OP2	21 31.500	39 13.470	26.2M	978768.39	978742.61	33.87	30.93	0.00	0.00	0.04	30.90	0.35	OP2
Q4	21 29.870	39 14.370	29.8M	978754.28	978740.94	22.53	19.20	0.00	0.00	0.04	19.16	0.35	Q4
Q5	21 30.010	39 15.170	38.3M	978753.54	978741.09	24.27	19.99	0.00	0.00	0.06	19.93	0.35	Q5
R6	21 29.040	39 15.660	44.7M	978746.69	978740.10	20.39	15.39	0.00	0.00	0.06	15.32	0.48	R6
R5	21 28.810	39 14.300	29.7M	978750.05	978739.86	19.36	16.03	0.00	0.00	0.04	15.99	0.35	R5
R4	21 28.580	39 13.150	20.8M	978756.74	978739.63	23.53	21.21	0.00	0.00	0.03	21.17	0.35	R4
P4	21 30.560	39 11.570	10.0M	978754.68	978741.65	16.11	14.99	0.00	0.00	0.01	14.98	0.58	P4
JB2	21 31.330	39 10.580	7.6M	978753.44	978742.44	13.35	12.50	0.00	0.00	0.01	12.49	0.21	JB2
JB2	21 31.330	39 10.580	7.6M	978753.44	978742.44	13.35	12.50	0.00	0.00	0.01	12.49	0.21	JB2
R1	21 27.970	39 9.450	4.9M	978751.24	978739.00	13.75	13.20	0.00	0.00	0.01	13.20	0.35	R1
R2	21 27.890	39 10.300	4.5M	978752.67	978738.92	15.14	14.63	0.00	0.00	0.01	14.63	0.35	R2
R3	21 28.350	39 11.780	12.7M	978758.01	978739.39	22.54	21.12	0.00	0.00	0.02	21.10	0.35	R3
QR1	21 28.870	39 11.450	12.3M	978756.45	978739.92	20.33	18.95	0.00	0.00	0.02	18.93	0.64	QR1
R4	21 28.580	39 13.150	20.8M	978756.68	978739.63	23.48	21.15	0.00	0.00	0.03	21.12	0.35	R4
JB2	21 31.330	39 10.580	7.6M	978753.44	978742.44	13.35	12.50	0.00	0.00	0.01	12.49	0.21	JB2
JB2	21 31.330	39 10.580	7.6M	978753.44	978742.44	13.35	12.50	0.00	0.00	0.01	12.49	0.21	JB2
A1	21 46.020	39 3.200	0.0M	978774.49	978757.54	16.95	16.95	0.00	0.00	0.00	16.95	0.16	A1
A2	21 46.380	39 4.420	1.0M	978778.14	978757.92	20.53	20.42	0.00	0.00	0.00	20.42	0.38	A2
A3	21 46.860	39 5.750	0.2M	978777.01	978758.41	18.66	18.64	0.00	0.00	0.00	18.64	0.42	A3
A4	21 46.930	39 6.810	3.0M	978773.66	978758.48	16.10	15.77	0.00	0.00	0.00	15.76	0.67	A4
A5	21 47.350	39 8.240	3.6M	978769.70	978758.92	11.89	11.49	0.00	0.00	0.01	11.48	0.42	A5
A6	21 47.760	39 9.750	8.5M	978769.16	978759.34	12.45	11.49	0.00	0.00	0.01	11.48	0.48	A6
B7	21 46.880	39 10.960	15.7M	978772.76	978758.43	19.17	17.41	0.00	0.00	0.02	17.39	0.35	B7
B8	21 47.220	39 12.240	15.5M	978775.38	978758.78	21.39	19.65	0.00	0.00	0.02	19.63	1.26	B8
B6	21 46.500	39 9.290	4.6M	978765.87	978758.04	9.25	8.74	0.00	0.00	0.01	8.73	0.38	B6
B5	21 46.260	39 8.150	1.6M	978768.46	978757.79	11.16	10.98	0.00	0.00	0.00	10.98	0.45	B5
B4	21 45.940	39 7.130	2.2M	978769.97	978757.46	13.18	12.94	0.00	0.00	0.00	12.93	0.42	B4
B3	21 45.720	39 6.010	3.3M	978772.63	978757.23	16.41	16.04	0.00	0.00	0.00	16.04	0.35	B3
B2	21 45.350	39 4.740	3.7M	978773.31	978756.85	17.60	17.18	0.00	0.00	0.01	17.18	0.35	B2
B1	21 45.160	39 3.860	0.0M	978772.58	978756.66	15.92	15.92	0.00	0.00	0.00	15.92	0.16	B1
C1	21 44.170	39 4.500	2.2M	978770.29	978755.63	15.33	15.09	0.00	0.00	0.00	15.08	0.35	C1

Appendix--*Principal facts for the 215 gravity stations used in the gravity survey of the greater Jiddah area*

ID	LAT	LONG	ELEV	OG	THG	FAA	SBA	HTC	TTC	CC	CBA	S.D.CBA	ID
C2	21 44.440	39 5.640	4.0M	978771.55	978755.91	16.87	16.42	0.00	0.00	0.01	16.42	0.35	C2
C3	21 44.660	39 6.650	4.1M	978768.33	978756.14	13.45	13.00	0.00	0.00	0.01	12.99	0.35	C3
CD1	21 44.380	39 7.680	2.7M	978765.31	978755.85	10.29	9.99	0.00	0.00	0.00	9.98	0.35	CD1
C4	21 45.060	39 8.130	2.2M	978765.56	978756.55	9.69	9.44	0.00	0.00	0.00	9.44	0.35	C4
C5	21 45.210	39 9.160	6.5M	978763.78	978756.71	9.08	8.35	0.00	0.00	0.01	8.34	0.35	C5
C6	21 45.440	39 10.050	13.0M	978762.92	978756.95	9.99	8.54	0.00	0.00	0.02	8.52	0.35	C6
C7	21 45.660	39 10.950	21.5M	978768.77	978757.17	18.23	15.83	0.00	0.00	0.03	15.80	0.35	C7
C8	21 46.110	39 11.750	29.1M	978773.03	978757.64	24.38	21.12	0.00	0.00	0.04	21.08	0.35	C8
C9	21 46.240	39 13.970	38.7M	978771.77	978757.77	25.95	21.62	0.00	0.00	0.06	21.56	0.48	C9
C10	21 46.640	39 14.260	52.9M	978767.21	978758.18	25.35	19.43	0.00	0.00	0.08	19.36	0.38	C10
D2	21 43.320	39 5.700	6.9M	978769.58	978754.76	16.96	16.18	0.00	0.00	0.01	16.17	0.35	D2
D1	21 43.090	39 5.010	0.0M	978768.08	978754.52	13.56	13.56	0.00	0.00	0.00	13.56	0.16	D1
JB2	21 31.330	39 10.580	7.6M	978753.44	978742.44	13.35	12.50	0.00	0.00	0.01	12.49	0.21	JB2
JB2	21 31.330	39 10.580	7.6M	978753.44	978742.44	13.35	12.50	0.00	0.00	0.01	12.49	0.21	JB2
D1	21 43.090	39 5.010	0.0M	978766.52	978754.52	12.00	12.00	0.00	0.00	0.00	12.00	0.16	D1
D3	21 43.230	39 6.710	0.0M	978766.89	978754.66	12.23	12.23	0.00	0.00	0.00	12.23	0.16	D3
D4	21 43.850	39 7.840	2.0M	978764.30	978755.30	9.61	9.39	0.00	0.00	0.00	9.39	0.35	D4
D5	21 44.080	39 8.920	2.0M	978761.90	978755.54	6.98	6.75	0.00	0.00	0.00	6.75	0.35	D5
D6	21 44.320	39 10.090	5.0M	978761.22	978755.79	6.97	6.42	0.00	0.00	0.01	6.41	0.35	D6
D7	21 44.590	39 11.200	14.5M	978768.18	978756.07	16.59	14.97	0.00	0.00	0.02	14.95	0.35	D7
D8	21 44.940	39 12.440	26.0M	978769.98	978756.43	21.58	18.67	0.00	0.00	0.04	18.63	0.35	D8
D9	21 45.180	39 13.600	38.9M	978765.81	978756.68	21.14	16.79	0.00	0.00	0.06	16.73	0.35	D9
D10	21 45.440	39 14.750	51.8M	978760.87	978756.95	19.91	14.12	0.00	0.00	0.07	14.04	0.42	D10
E9	21 44.430	39 15.030	76.5M	978754.17	978755.90	21.89	13.33	0.00	0.00	0.11	13.22	0.42	E9
E8	21 44.260	39 13.850	47.5M	978761.57	978755.73	20.51	15.19	0.00	0.00	0.07	15.12	0.35	E8
E7	21 43.800	39 12.820	30.4M	978765.28	978755.25	19.41	16.01	0.00	0.00	0.04	15.96	0.38	E7
E6	21 43.600	39 11.400	15.0M	978767.40	978755.05	16.98	15.31	0.00	0.00	0.02	15.28	0.35	E6
E5	21 43.270	39 10.410	7.7M	978761.36	978754.71	9.03	8.17	0.00	0.00	0.01	8.16	0.35	E5
E4	21 42.880	39 8.880	2.4M	978760.65	978754.30	7.09	6.82	0.00	0.00	0.00	6.82	0.35	E4
E3	21 42.630	39 7.780	2.5M	978762.64	978754.05	9.37	9.09	0.00	0.00	0.00	9.08	0.35	E3
E2	21 42.090	39 6.530	3.2M	978766.19	978753.49	13.69	13.33	0.00	0.00	0.00	13.33	0.35	E2
F1	21 40.830	39 5.710	0.0M	978763.77	978752.19	11.58	11.58	0.00	0.00	0.00	11.58	0.16	F1
F2	21 41.210	39 7.030	1.7M	978763.69	978752.58	11.63	11.44	0.00	0.00	0.00	11.44	0.42	F2
F3	21 41.680	39 8.430	6.2M	978760.67	978753.07	9.52	8.83	0.00	0.00	0.01	8.82	0.35	F3
F4	21 41.830	39 9.540	6.2M	978760.08	978753.22	8.77	8.07	0.00	0.00	0.01	8.07	0.35	F4
F5	21 42.250	39 10.830	14.3M	978764.70	978753.65	15.46	13.86	0.00	0.00	0.02	13.84	0.35	F5
F6	21 42.770	39 12.340	31.1M	978767.61	978754.19	23.02	19.54	0.00	0.00	0.05	19.50	0.42	F6
F7	21 42.740	39 13.240	40.6M	978766.36	978754.16	24.73	20.19	0.00	0.00	0.06	20.13	0.35	F7
F8	21 43.150	39 14.400	55.0M	978760.31	978754.58	22.71	16.55	0.00	0.00	0.08	16.48	0.35	F8
F9	21 43.630	39 15.260	67.9M	978755.35	978755.08	21.23	13.63	0.00	0.00	0.10	13.54	0.54	F9
G9	21 42.180	39 15.620	78.6M	978754.24	978753.58	24.92	16.13	0.00	0.00	0.11	16.02	0.67	G9
G8	21 41.850	39 14.460	58.1M	978761.06	978753.24	25.75	19.25	0.00	0.00	0.08	19.17	0.84	G8
G7	21 41.550	39 13.420	45.7M	978769.03	978752.93	30.20	25.09	0.00	0.00	0.07	25.02	0.87	G7
G6	21 41.340	39 12.340	33.8M	978770.45	978752.72	28.17	24.38	0.00	0.00	0.05	24.34	0.80	G6
G5	21 41.030	39 11.020	17.1M	978768.36	978752.40	21.24	19.33	0.00	0.00	0.02	19.30	0.58	G5
G4	21 40.670	39 9.550	9.1M	978758.96	978752.03	9.75	8.73	0.00	0.00	0.01	8.71	0.35	G4
G3	21 40.430	39 8.000	5.7M	978760.54	978751.78	10.52	9.88	0.00	0.00	0.01	9.88	0.35	G3
JB2	21 31.330	39 10.580	7.6M	978753.44	978742.44	13.35	12.50	0.00	0.00	0.01	12.49	0.21	JB2
JB2	21 31.330	39 10.580	7.6M	978753.44	978742.44	13.35	12.50	0.00	0.00	0.01	12.49	0.21	JB2
G2	21 40.130	39 7.050	6.6M	978763.26	978751.47	13.83	13.09	0.00	0.00	0.01	13.08	0.35	G2
G1	21 39.850	39 6.980	2.3M	978763.10	978751.18	12.63	12.37	0.00	0.00	0.00	12.37	0.35	G1

Appendix--*Principal facts for the 215 gravity stations used in the gravity survey of the greater Jiddah area*--Continued

ID	LAT	LONG	ELEV	OG	THG	FAA	SBA	HTC	TTC	CC	CBA	S.D.CBA	ID
H1	21 38.900	39 6.180	2.4M	978762.21	978750.21	12.74	12.47	0.00	0.00	0.00	12.47	0.12	H1
H2	21 39.120	39 7.380	9.1M	978762.30	978750.43	14.68	13.66	0.00	0.00	0.01	13.65	0.35	H2
H3	21 39.340	39 8.650	10.4M	978759.97	978750.66	12.52	11.36	0.00	0.00	0.02	11.34	0.35	H3
H4	21 39.680	39 10.050	14.4M	978762.23	978751.01	15.67	14.06	0.00	0.00	0.02	14.04	0.35	H4
H5	21 39.960	39 11.110	23.4M	978769.99	978751.30	25.92	23.30	0.00	0.00	0.03	23.27	0.35	H5
H6	21 40.330	39 12.740	40.9M	978769.34	978751.68	30.28	25.71	0.00	0.00	0.06	25.65	0.51	H6
H7	21 40.420	39 13.620	67.7M	978763.96	978751.77	33.09	25.51	0.00	0.00	0.10	25.42	0.51	H7
H8	21 40.800	39 14.940	82.0M	978754.74	978752.16	27.90	18.72	0.00	0.00	0.12	18.60	0.45	H8
H9	21 40.770	39 15.090	148.5M	978736.27	978752.13	29.98	13.37	0.00	0.00	0.21	13.16	0.54	H9
I8	21 39.860	39 15.970	80.8M	978748.50	978751.19	22.25	13.21	0.00	0.00	0.12	13.10	0.87	I8
I7	21 39.770	39 15.130	67.6M	978754.24	978751.10	24.01	16.44	0.00	0.00	0.10	16.35	0.87	I7
I6	21 39.490	39 14.140	59.0M	978764.05	978750.81	31.45	24.85	0.00	0.00	0.09	24.76	0.80	I6
I5B	21 39.180	39 12.870	45.2M	978767.89	978750.49	31.36	26.30	0.00	0.00	0.07	26.23	0.97	I5B
I5A	21 38.930	39 11.630	30.1M	978773.09	978750.24	32.15	28.78	0.00	0.00	0.04	28.73	1.10	I5A
I4	21 38.620	39 10.400	18.4M	978765.11	978749.92	20.87	18.81	0.00	0.00	0.03	18.78	0.80	I4
I3	21 38.160	39 9.170	10.5M	978759.72	978749.44	13.52	12.34	0.00	0.00	0.02	12.33	1.06	I3
I2	21 37.890	39 7.890	8.6M	978760.41	978749.17	13.90	12.93	0.00	0.00	0.01	12.92	0.51	I2
I1	21 37.980	39 6.300	1.8M	978761.51	978749.26	12.81	12.61	0.00	0.00	0.00	12.60	0.70	I1
J1	21 36.340	39 6.480	4.7M	978760.32	978747.57	14.20	13.67	0.00	0.00	0.01	13.67	0.58	J1
J2	21 36.440	39 7.240	8.6M	978761.19	978747.68	16.17	15.21	0.00	0.00	0.01	15.20	0.77	J2
J3	21 36.630	39 8.470	5.9M	978758.70	978747.87	12.65	11.99	0.00	0.00	0.01	11.98	0.35	J3
J4	21 37.160	39 9.510	11.6M	978760.13	978748.42	15.30	14.00	0.00	0.00	0.02	13.98	0.74	J4
JB2	21 31.330	39 10.580	7.6M	978753.44	978742.44	13.35	12.50	0.00	0.00	0.01	12.49	0.21	JB2
JB2	21 31.330	39 10.580	7.6M	978753.44	978742.44	13.35	12.50	0.00	0.00	0.01	12.49	0.21	JB2
J5	21 37.500	39 10.550	12.0M	978766.72	978748.77	21.65	20.31	0.00	0.00	0.02	20.29	0.35	J5
J6	21 37.900	39 12.160	26.6M	978771.77	978749.18	30.81	27.83	0.00	0.00	0.04	27.79	0.38	J6
J7	21 38.000	39 13.100	37.7M	978767.10	978749.28	29.46	25.24	0.00	0.00	0.05	25.18	0.35	J7
J8	21 38.380	39 14.280	51.1M	978760.46	978749.67	26.57	20.85	0.00	0.00	0.07	20.77	0.35	J8
J9	21 38.620	39 15.400	63.5M	978752.80	978749.92	22.48	15.38	0.00	0.00	0.09	15.28	0.35	J9
J10	21 38.740	39 16.550	85.7M	978744.61	978750.04	21.02	11.44	0.00	0.00	0.12	11.31	0.35	J10
K10	21 37.660	39 16.770	85.5M	978745.22	978748.93	22.69	13.12	0.00	0.00	0.12	13.00	0.35	K10
K9	21 37.490	39 15.940	83.3M	978748.03	978748.76	24.99	15.67	0.00	0.00	0.12	15.55	0.35	K9
K8	21 37.230	39 14.400	47.3M	978762.37	978748.49	28.48	23.19	0.00	0.00	0.07	23.12	0.45	K8
K7	21 36.990	39 13.190	33.5M	978767.45	978748.24	29.55	25.80	0.00	0.00	0.05	25.75	0.35	K7
K6	21 36.540	39 11.930	24.0M	978768.10	978747.78	27.73	25.05	0.00	0.00	0.03	25.01	0.35	K6
K5	21 36.150	39 10.700	17.2M	978763.71	978747.38	21.64	19.72	0.00	0.00	0.03	19.69	0.35	K5
K4	21 36.100	39 9.730	6.9M	978759.75	978747.33	14.56	13.78	0.00	0.00	0.01	13.77	0.35	K4
K3	21 35.500	39 8.740	2.4M	978757.12	978746.71	11.15	10.88	0.00	0.00	0.00	10.88	0.35	K3
K2	21 35.500	39 7.450	1.1M	978760.73	978746.71	14.36	14.23	0.00	0.00	0.00	14.23	0.35	K2
K1	21 35.150	39 6.440	0.0M	978758.89	978746.35	12.54	12.54	0.00	0.00	0.00	12.54	0.16	K1
M5	21 34.700	39 13.210	36.8M	978765.38	978745.89	30.85	26.73	0.00	0.00	0.05	26.68	0.35	M5
M6	21 34.840	39 15.650	46.9M	978761.36	978746.04	29.80	24.56	0.00	0.00	0.07	24.49	0.70	M6
M7	21 35.170	39 16.230	72.5M	978753.01	978746.37	29.02	20.91	0.00	0.00	0.10	20.80	0.74	M7
N10	21 34.300	39 17.790	73.4M	978749.56	978745.48	26.74	18.53	0.00	0.00	0.11	18.42	0.77	N10
M8	21 35.640	39 17.470	86.7M	978747.27	978746.86	27.18	17.48	0.00	0.00	0.12	17.35	0.67	M8
N9	21 34.110	39 16.370	67.2M	978753.72	978745.29	29.18	21.66	0.00	0.00	0.10	21.56	0.80	N9
N8	21 33.900	39 15.380	87.3M	978753.56	978745.07	35.44	25.67	0.00	0.00	0.13	25.54	0.90	N8
N7	21 33.720	39 14.410	44.6M	978762.19	978744.89	31.07	26.08	0.00	0.00	0.06	26.01	0.77	N7
N6	21 33.340	39 13.050	31.7M	978766.68	978744.50	31.97	28.42	0.00	0.00	0.05	28.37	0.51	N6
JB2	21 31.330	39 10.580	7.6M	978753.42	978742.44	13.32	12.47	0.00	0.00	0.01	12.46	0.35	JB2

Appendix--*Principal facts for the 215 gravity stations used in the gravity survey of the greater Jiddah area*--Continued

ID	LAT	LONG	ELEV	OG	THG	FAA	SBA	HTC	TTC	CC	CBA	S.D.CBA	ID
S7	21 28.380	39 16.800	58.1M	978743.76	978739.42	22.27	15.77	0.00	0.00	0.08	15.69	0.35	S7
S8	21 28.680	39 18.240	79.4M	978743.01	978739.73	27.80	18.91	0.00	0.00	0.11	18.80	0.54	S8
S9	21 28.700	39 19.280	100.3M	978739.18	978739.75	30.40	19.17	0.00	0.00	0.14	19.03	0.51	S9
T9	21 27.870	39 19.560	106.8M	978735.99	978738.90	30.06	18.11	0.00	0.00	0.15	17.96	0.87	T9
T8	21 27.500	39 18.420	79.5M	978740.51	978738.52	26.53	17.64	0.00	0.00	0.11	17.52	0.35	T8
T7	21 27.300	39 17.300	78.6M	978740.01	978738.32	25.96	17.16	0.00	0.00	0.11	17.05	0.35	T7
U8	21 26.140	39 17.600	55.7M	978742.14	978737.13	22.20	15.97	0.00	0.00	0.08	15.88	0.61	U8
U9	21 26.380	39 18.770	74.4M	978738.76	978737.38	24.35	16.03	0.00	0.00	0.11	15.92	0.35	U9
U10	21 26.410	39 19.900	92.1M	978735.51	978737.41	26.53	16.22	0.00	0.00	0.13	16.09	0.35	U10
UV6	21 25.750	39 18.950	90.0M	978736.82	978736.74	27.86	17.79	0.00	0.00	0.13	17.66	0.42	UV6
UV5	21 25.440	39 17.780	68.7M	978741.46	978736.42	26.25	18.56	0.00	0.00	0.10	18.46	0.35	UV5
UV4	21 25.170	39 16.590	68.0M	978742.77	978736.14	27.62	20.01	0.00	0.00	0.10	19.91	0.61	UV4
U7	21 25.840	39 16.410	64.7M	978743.23	978736.83	26.37	19.13	0.00	0.00	0.09	19.04	0.61	U7
UV3	21 24.960	39 15.340	32.6M	978751.73	978735.93	25.87	22.22	0.00	0.00	0.05	22.17	1.13	UV3
U6	21 25.700	39 14.900	33.0M	978754.42	978736.69	27.92	24.23	0.00	0.00	0.05	24.18	1.89	U6
U5	21 25.260	39 13.420	21.4M	978754.26	978736.24	24.63	22.23	0.00	0.00	0.03	22.20	0.80	U5
UV2	21 24.590	39 13.710	12.0M	978752.33	978735.55	20.48	19.14	0.00	0.00	0.02	19.12	0.51	UV2
U4	21 24.700	39 12.290	4.2M	978752.59	978735.67	18.23	17.76	0.00	0.00	0.01	17.75	0.35	U4
UV1	21 24.180	39 11.600	1.0M	978750.36	978735.14	15.53	15.42	0.00	0.00	0.00	15.42	0.61	UV1
S1	21 26.100	39 8.770	0.0M	978750.18	978737.09	13.08	13.08	0.00	0.00	0.00	13.08	0.16	S1
JB2	21 31.330	39 10.580	7.6M	978753.44	978742.44	13.35	12.50	0.00	0.00	0.01	12.49	0.35	JB2
JB2	21 31.330	39 10.580	7.6M	978753.44	978742.44	13.35	12.50	0.00	0.00	0.01	12.49	0.35	JB2
TU2	21 25.030	39 10.990	4.1M	978750.95	978736.00	16.22	15.76	0.00	0.00	0.01	15.75	0.45	TU2
U3	21 24.280	39 11.800	4.1M	978749.26	978735.24	15.29	14.83	0.00	0.00	0.01	14.83	0.45	U3
U0	21 23.440	39 9.670	3.1M	978747.34	978734.38	13.92	13.57	0.00	0.00	0.00	13.56	0.54	U0
U1	21 23.930	39 9.070	3.0M	978747.92	978734.88	13.96	13.63	0.00	0.00	0.00	13.62	0.54	U1
U1A	21 24.040	39 9.540	4.1M	978748.24	978734.99	14.51	14.05	0.00	0.00	0.01	14.05	0.16	U1A
TU1	21 24.650	39 9.970	3.3M	978748.33	978735.61	13.73	13.36	0.00	0.00	0.00	13.36	0.67	TU1
CD1	21 44.380	39 7.680	2.7M	978765.47	978755.85	10.45	10.15	0.00	0.00	0.00	10.15	0.35	CD1
A8	21 48.300	39 12.120	29.8M	978771.17	978759.90	20.47	17.13	0.00	0.00	0.04	17.09	0.35	A8
A9	21 48.560	39 14.460	46.1M	978768.49	978760.17	22.56	17.40	0.00	0.00	0.07	17.33	0.35	A9
B9	21 47.650	39 13.920	47.9M	978771.78	978759.23	27.33	21.97	0.00	0.00	0.07	21.91	0.35	B9
F8	21 43.150	39 14.400	55.0M	978760.15	978754.58	22.55	16.39	0.00	0.00	0.08	16.32	0.35	F8
JB2	21 31.330	39 10.580	7.6M	978753.44	978742.44	13.35	12.50	0.00	0.00	0.01	12.49	0.21	JB2
JB2	21 31.330	39 10.580	7.6M	978753.44	978742.44	13.35	12.50	0.00	0.00	0.01	12.49	0.21	JB2
S2	21 26.830	39 10.810	6.8M	978752.91	978737.84	17.17	16.41	0.00	0.00	0.01	16.40	0.35	S2
S3	21 27.200	39 11.800	5.7M	978755.16	978738.22	18.71	18.07	0.00	0.00	0.01	18.06	0.35	S3
S4	21 27.450	39 13.260	20.0M	978760.11	978738.47	27.81	25.57	0.00	0.00	0.03	25.55	0.35	S4
S5	21 27.900	39 14.420	29.0M	978749.95	978738.93	19.97	16.73	0.00	0.00	0.04	16.69	0.35	S5
T3	21 26.050	39 11.710	7.7M	978755.05	978737.04	20.39	19.52	0.00	0.00	0.01	19.51	0.45	T3
S6	21 28.120	39 15.610	42.1M	978745.57	978739.16	19.41	14.70	0.00	0.00	0.06	14.64	0.35	S6
JB2	21 31.330	39 10.580	7.6M	978753.33	978742.44	13.24	12.39	0.00	0.00	0.01	12.38	0.21	JB2

Appendix--*Principal facts for the 215 gravity stations used in the gravity survey of the greater Jiddah area*--Continued

Stations established with LaCoste-Ramberg gravimeter G328														
ID	LAT	LONG	ELEV	OG	THG	FAA	SBA	HTC	TTC	CC	CBA	S.D.CBA	ID
JB2	21 31.330	39 10.580	7.6M	978753.44	978742.44	13.35	12.50	0.00	0.00	0.01	12.49	0.35	JB2
L1	21 34.050	39 6.600	0.0M	978757.87	978745.22	12.65	12.65	0.00	0.00	0.00	12.65	0.16	L1
L2	21 34.420	39 7.940	2.0M	978758.65	978745.60	13.66	13.44	0.00	0.00	0.00	13.43	0.67	L2
L3	21 34.660	39 9.030	3.0M	978755.80	978745.85	10.87	10.54	0.00	0.00	0.00	10.53	0.67	L3
L4	21 35.040	39 10.370	8.3M	978757.14	978746.24	13.46	12.53	0.00	0.00	0.01	12.52	0.35	L4
L5	21 35.180	39 11.140	18.6M	978764.76	978746.38	24.11	22.03	0.00	0.00	0.03	22.01	0.42	L5
L6	21 35.640	39 12.800	20.8M	978766.71	978746.86	26.28	23.95	0.00	0.00	0.03	23.92	0.35	L6
L7	21 35.860	39 13.930	31.1M	978764.95	978747.08	27.47	23.99	0.00	0.00	0.05	23.95	0.35	L7
L8	21 36.160	39 15.240	45.7M	978756.32	978747.39	23.04	17.92	0.00	0.00	0.07	17.86	0.35	L8
L9	21 36.770	39 16.980	69.1M	978748.51	978748.02	21.83	14.09	0.00	0.00	0.10	14.00	0.35	L9
O10	21 33.390	39 18.020	80.6M	978745.10	978744.55	25.43	16.42	0.00	0.00	0.12	16.30	0.35	O10
O9	21 32.970	39 17.210	85.7M	978745.14	978744.12	27.48	17.89	0.00	0.00	0.12	17.77	0.48	O9
O8	21 32.860	39 16.000	74.7M	978751.51	978744.01	30.56	22.20	0.00	0.00	0.11	22.10	0.35	O8
P5	21 31.450	39 15.100	38.9M	978759.22	978742.56	28.66	24.31	0.00	0.00	0.06	24.25	1.39	P5
P6	21 31.750	39 16.300	50.9M	978750.53	978742.87	23.38	17.68	0.00	0.00	0.07	17.61	0.45	P6
P7	21 31.980	39 17.430	62.9M	978746.53	978743.10	22.85	15.81	0.00	0.00	0.09	15.72	0.35	P7
P8	21 32.250	39 18.350	82.0M	978741.57	978743.38	23.51	14.33	0.00	0.00	0.12	14.21	0.35	P8
Q8	21 31.130	39 18.660	82.2M	978743.45	978742.23	26.59	17.39	0.00	0.00	0.12	17.28	1.10	Q8
Q7	21 31.130	39 17.600	64.2M	978744.55	978742.23	22.13	14.95	0.00	0.00	0.09	14.86	0.35	Q7
Q6	21 30.770	39 16.170	55.3M	978748.67	978741.87	23.88	17.69	0.00	0.00	0.08	17.61	0.35	Q6
R7	21 29.630	39 16.750	56.0M	978748.52	978740.70	25.10	18.84	0.00	0.00	0.08	18.76	0.35	R7
R8	21 29.770	39 18.050	75.5M	978743.62	978740.84	26.09	17.64	0.00	0.00	0.11	17.53	0.35	R8
R9	21 29.970	39 19.030	92.5M	978739.01	978741.05	26.52	16.17	0.00	0.00	0.13	16.03	0.35	R9
JB2	21 31.330	39 10.580	7.6M	978753.44	978742.44	13.35	12.50	0.00	0.00	0.01	12.49	0.21	JB2
JB2	21 31.330	39 10.580	7.6M	978753.44	978742.44	13.35	12.50	0.00	0.00	0.01	12.49	0.21	JB2
T1	21 25.830	39 9.550	0.6M	978749.53	978736.82	12.90	12.83	0.00	0.00	0.00	12.83	0.23	T1
T2	21 25.750	39 10.630	1.9M	978751.15	978736.74	15.00	14.79	0.00	0.00	0.00	14.78	0.35	T2
T4	21 26.160	39 13.100	13.0M	978757.21	978737.15	24.07	22.61	0.00	0.00	0.02	22.59	0.35	T4
T5	21 26.770	39 14.870	28.9M	978750.49	978737.78	21.63	18.40	0.00	0.00	0.04	18.36	0.67	T5
T6	21 27.180	39 15.850	39.9M	978745.37	978738.20	19.49	15.03	0.00	0.00	0.06	14.97	0.77	T6